

Chemical Science

Accepted Manuscript

This article can be cited before page numbers have been issued, to do this please use: Q. Liang, B. Fan, W. Jin, Y. Liu, D. Su, P. Chen, J. Yoon, B. Tang and G. Chen, *Chem. Sci.*, 2026, DOI: 10.1039/D6SC02520J.



This is an Accepted Manuscript, which has been through the Royal Society of Chemistry peer review process and has been accepted for publication.

Accepted Manuscripts are published online shortly after acceptance, before technical editing, formatting and proof reading. Using this free service, authors can make their results available to the community, in citable form, before we publish the edited article. We will replace this Accepted Manuscript with the edited and formatted Advance Article as soon as it is available.

You can find more information about Accepted Manuscripts in the [Information for Authors](#).

Please note that technical editing may introduce minor changes to the text and/or graphics, which may alter content. The journal's standard [Terms & Conditions](#) and the [Ethical guidelines](#) still apply. In no event shall the Royal Society of Chemistry be held responsible for any errors or omissions in this Accepted Manuscript or any consequences arising from the use of any information it contains.

Clinical Fluorescent Probes: Mechanisms, Advantages and Inspirations

Qiao Liang^a, Baolei Fan^{*a}, Wenfang Jin^g, Yuxia Liu^{*b}, Dongliang Suⁱ, Pu Chen^{d,e*}, Juyoung Yoon^{c,h*}, Bo Tang^{f*}
and Guang Chen^{a,b*}

ADDRESS:

^a College of Pharmacy, Hubei University of Science and Technology, Xianning, 437000, China.

^b Shaanxi Key Laboratory of Chemical Additives for Industry, College of Chemistry and Chemical Engineering, Shaanxi University of Science and Technology, Xi'an 710021, China.

^c Department of Chemistry and Nano Science, Ewha Womans University, Seoul 03760, Republic of Korea

^d School of Chemical and Biomolecular Engineering, Eastern Institute of Technology, Ningbo, Zhejiang 315200, P. R. China.

^e Department of Chemical Engineering and Waterloo Institute for Nanotechnology University of Waterloo 200 University Avenue West, Waterloo, ON N2L3G1, Canada.

^f Laoshan Laboratory, Qingdao 266237, P. R. China.

^g Xian'an District Maternal and Child Health Hospital, Xianning, 437000, China.

^h Graduate Program in Innovative Biomaterials Convergence, Ewha Womans University, Seoul 03760, Korea.

ⁱ Yimingtai Biotechnology Co., Ltd, No. 507 Binhe Avenue, Development Zone, Taian 271200, China.

E-mail:

Baolei Fan: fanbl_1980@163.com;

Yuxia Liu: liuyuxia2008@163.com;

Pu Chen: p4chen@uwaterloo.ca;

Juyoung Yoon: jyoon@ewha.ac.kr

Bo Tang: tangb@sdnu.edu.cn;

Guang Chen: chenandguang@163.com



AbstractView Article Online
DOI: 10.1039/D6SC02520J

Fluorescence imaging is revolutionizing oncologic surgery by overcoming the limitations of visual and tactile guidance. Despite this promise, clinical translation remains limited, with only a handful of probes having received regulatory approval. Using a challenges–strategy–efficacy–comparison framework, this review outlines clinical probes used across six major organ systems (nervous, circulatory, respiratory, digestive, reproductive, and urinary), including: 1) clinical surgical challenges for probe design: tumor heterogeneity, occult margins, and deep-seated lesions; 2) strategy and mechanisms: spanning ligand targeting, specific activatable chemistries, deep-penetration molecular scaffolds, and theranostic integration; 3) clinical quantitative efficacy metrics: differentiated distinction, excellent biosafety, high signal-to-noise ratio, and operational compatibility, and 4) functional extension of probes beyond resection. Moreover, a comprehensive comparative analysis between clinical and non-clinical probes is conducted to highlight the gaps and challenges between them, whereby the insights from the advantages of clinical probes are discussed to inspire the development of next-generation fluorescent probes. Based on data from a large number of clinical trials and surgeon requirements, this review highlights the crucial role of fluorescent probes in tumor removal, providing guidance to accelerate their clinical translation.

Keywords

Fluorescent probes; Human clinical applications; Strategy and mechanisms; Clinical translation.



1 Introduction

Clinically, the treatment of tumors includes surgical resection, chemotherapy, radiotherapy, immunotherapy, targeted therapy, photodynamic therapy (PDT).¹⁻⁵ Among these, surgical resection stands out as the most effective and direct method.⁶ However, the location of tumors significantly influences the surgical approach and its efficiency. Tumors in different organs exhibit distinct characteristics, which include: 1) The size and depth of the tumor within normal tissues;⁷ 2) The number of tumors and tumor-positive lymph nodes;^{8, 9} 3) The distribution area of the tumors;¹⁰ 4) The speed and pathway of tumor metastasis;^{11, 12} 5) The extent of resection required for the tumors.¹³ These unique tumor features challenge surgeons. For instance, complex surgeries like craniotomy, cystoscopy, and lymph node dissection require extensive clinical experience, and surgeons often cannot rely on experience alone.¹⁴⁻¹⁶ Moreover, limited visual feedback and blind spots can cause unintentional tumor residues.¹⁷⁻¹⁹ Therefore, to enhance the outcomes of tumor surgical resection, new technologies and methods have been introduced in clinical practice.

Thankfully, the advancement of medical imaging technology has brought about improvements in tumor surgical procedures.²⁰⁻²⁴ Commonly used imaging techniques include magnetic resonance imaging (MRI), computed tomography (CT), positron emission computed tomography (PET), ultrasound imaging (US), and X-ray imaging.²⁵⁻²⁹ During the operation, surgeons can refer to the pre-operative images of the tumors to guide the resection process. Nonetheless, these imaging techniques come with many limitations, involving: lack of intraoperative real-time imaging, inaccurate discrimination of the tumor margin, low resolution, and radiation risks.³⁰⁻³² In light of these issues, there is an urgent need for a more efficient imaging method to further enhance the rate of complete tumor resection.

In recent years, ongoing molecular imaging advances have driven the development and use of fluorescent probes in tumor surgery.³³⁻³⁵ Fluorescence-guided surgery (FGS) holds great promise for tumor resection by providing real-time imaging and surgical guidance.^{36, 37} The process of FGS includes: 1) Administering fluorescent probes systemically (e.g., intravenous, oral) or topically (e.g., local injection, gargle);^{38, 39} 2) Probes enter tumor cells through inherent properties (lipophilicity, zwitterions) or targeting antibodies/ligands for precise tumor localization;^{40, 41} 3) Within tumor cells, probes emit fluorescence, enabling real-time tumor imaging during surgery;⁴² 4) Guided by fluorescence, surgeons can achieve complete tumor resection. Some probes, like photosensitizers, also kill tumor cells via PDT while guiding surgery.⁴³⁻⁴⁵ Theoretically, if fluorescent probes could precisely locate tumors and emit deep-penetrating fluorescence, such as near-infrared, they would represent an excellent strategy.⁴⁶ Regrettably, the development of probes is fraught with challenges, and there are only a limited number of fluorescent probes available for clinical use.⁴⁷ Although fluorescent probes for tumor imaging and guided surgery show great clinical promise, most probes are still in clinical trials, and full integration into patient treatment remains distant.^{48, 49} Therefore, a thorough discussion of the advantages and limitations of clinical probes, as well as the gap between non-clinical and clinical probes, is crucial for promoting their clinical translation.

Herein, we provide a comprehensive overview of clinically used fluorescent probes, following the clue of challenges–strategy–efficacy–comparison framework (Table 1). From the perspective of clinical application, we categorize the use of probes into six systems (nervous system, circulatory system, respiratory system, digestive system, reproductive system, and urinary system) to clearly analyze the specific requirements for probes in each. Emphasis is placed on the critical factors influencing probe design strategy and working mechanism. Representative case studies are discussed to illustrate how fluorescence-guided surgery reshapes operative strategies across diverse tumor types. Furthermore, we analyze the disparities between clinical and non-clinical probes, identifying both challenges and opportunities for researchers to address. We hope that this review will facilitate the translation of



non-clinical probes into clinical applications.

View Article Online
DOI: 10.1039/D6SC02520J

2 Clinical probes across organ systems

2.1 Clinical probes for nervous system

Due to the influence of certain unpredictable factors, the brain is prone to a prevalent form of cancer: glioma.⁵⁰ Regrettably, patients with glioma typically face a dismal prognosis and a high mortality rate.^{51, 52} While with the advancement of fluorescent probe, the fluorescence imaging has found clinical applications in guiding the resection of gliomas (Fig. 1A).⁵³

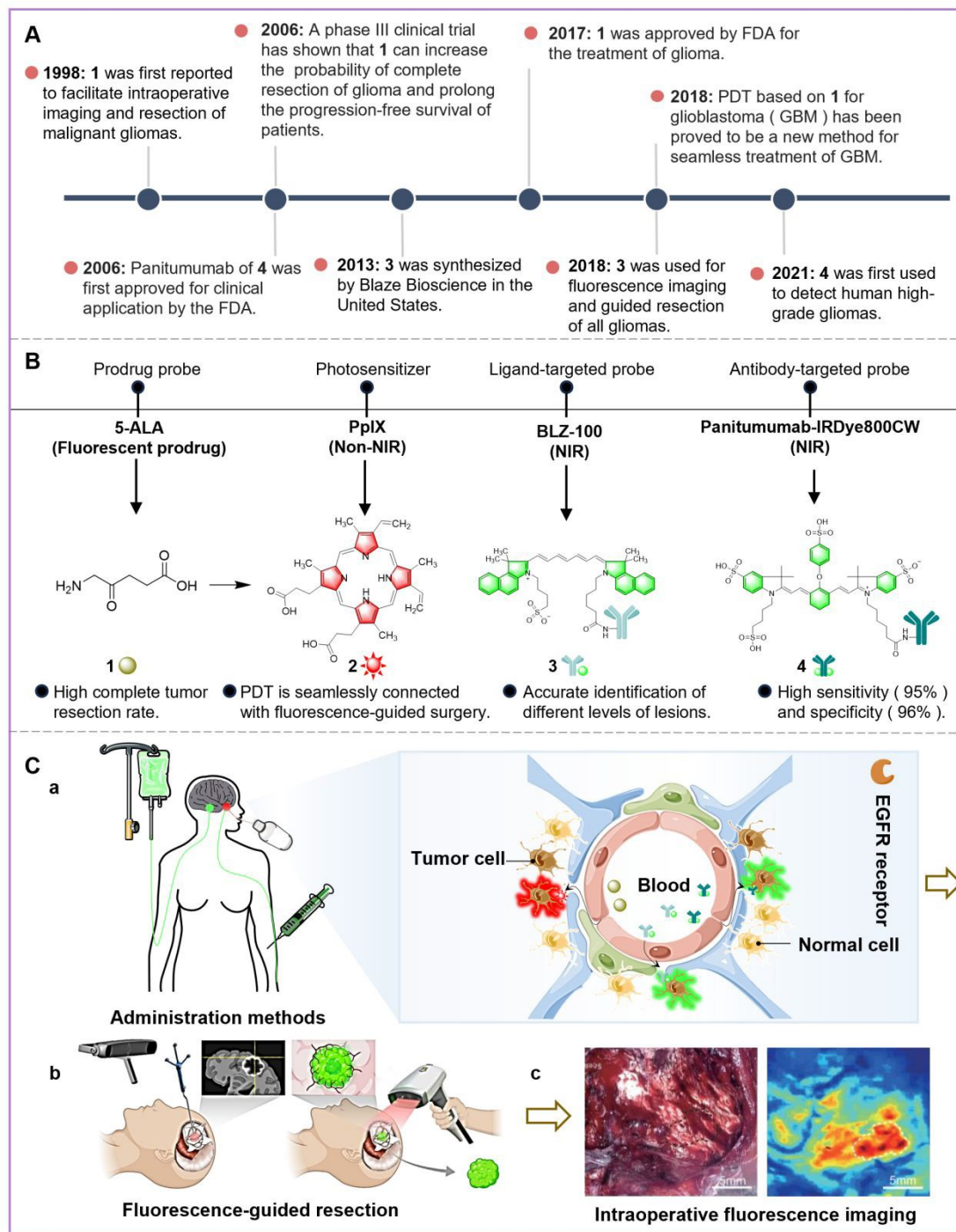


Fig. 1 (A) The timeline of research progress of fluorescent probes in the nervous system. (B) The chemical structures, categories, and clinical efficacies of the probes. (C) Administration methods, *in vivo* fluorescence mechanisms, intraoperative fluorescence-guided resection methods, and clinical fluorescence images during surgery of the probes. (C b) Reproduced from ref. 54 with permission from Ivyspring International Publisher, copyright 2021. (C c) Reproduced from ref. 48 with permission from Ivyspring International Publisher, copyright 2024.



2.1.1 Clinical probes for Brain

High-grade gliomas (grades III-IV) exhibit strong invasiveness, while conventional imaging (MRI/CT/US) lacks real-time guidance.⁵⁵⁻⁵⁸ Fluorescent probe **1** was employed in a phase III clinical trial.⁵⁹ The tumor-targeting and fluorescence properties of **1** are determined by its molecular structure and metabolism (Fig. 1B). Under physiological conditions, the amino group of **1** is protonated ($-\text{NH}_3^+$) and the carboxyl group is deprotonated ($-\text{COO}^-$), forming a zwitterionic structure. This conformation highly mimics short-peptide substrates of PEPT1/2, thereby enabling efficient internalization into tumor cells via highly expressed PEPT1/2-mediated active transport. After it enters tumor cells via PEPT1/2 transporters, it is enzymatically converted to protoporphyrin IX (PpIX: probe **2**), and accumulates in tumors with low ferrochelatase activity, emitting red fluorescence (635 nm) for real-time surgical visualization (Fig. 1C a, c).⁶⁰ Based on these properties, this phase III clinical strategy for fluorescence-guided surgery (FGS) improved outcomes: resection rates increased from 36% to 65%, recurrence was reduced, and 6-month progression-free survival doubled from 21.1% to 41%, with confirmed safety. Even for highly malignant glioblastoma (GBM, grade IV), combining probe **1**-guided surgery with post-resection photodynamic therapy, in which light-activated compound **2** generates reactive oxygen species, allows complete tumor removal.⁶¹

Compared with experimental probes in preclinical studies, we found probe **1** shows better clinical performance because it has high target specificity, proven therapeutic effects, and an established safety profile. These advantages also highlight key limitations of non-clinical probes: 1) Most experimental probes, such as macromolecular nanoparticles and antibody conjugates, have poor blood-brain barrier (BBB) penetration, whereas probe **1** uses small-molecule transporters for targeted delivery, suggesting that smaller probes can overcome this barrier. 2) Clinical gliomas are highly heterogeneous, which can cause false negatives when probes target variable receptors or enzymes. While probe **1** avoids this problem by using the universal heme synthesis pathway, and rational modifications, such as replacing 5-ALA's terminal carboxyl with a phosphonate ($\text{P}=\text{O}$) while keeping the γ -ketoglutarate backbone, can improve transporter recognition. 3) Experimental probes can cause accumulative toxicity in the organs. In contrast, Probe **1** is naturally metabolized via the protoporphyrin IX-heme pathway. It accumulates as protoporphyrin IX in tumor cells to generate fluorescence, but is rapidly converted to heme in normal cells. The small fraction of unincorporated probe **1** is quickly cleared by the kidneys.

Despite the satisfying clinical performance of probe **1**, current fluorescent probes still face challenges such as limited tumor selectivity, shallow tissue penetration, and insufficient signal in low-grade gliomas.^{62, 63} To overcome these challenges, probe **3**, the first clinical-grade probe combining targeting capability with near-infrared (NIR) fluorescence, was developed by conjugating chlorotoxin peptides with the NIR fluorophore indocyanine green (ICG) (Fig. 1B).⁶⁴ Probe **3**'s molecular structure and design strategy confer its key properties: conjugation of chlorotoxin peptides with the NIR fluorophore ICG enables selective binding to the chloride channel-3 (ClC-3), precise identification of neuroectodermal tumors such as gliomas and medulloblastomas, as well as the inhibition of chloride efflux-mediated metastasis. Its NIR fluorescence at 822 nm provides approximately 10 mm tissue penetration, achieving detection rates of 88% in high-grade (III/IV) and 50% in low-grade (I/II) gliomas, outperforming non-targeted probes like fluorescein and ICG. By leveraging these structure-defined properties, the clinical strategy of fluorescence-guided surgery with probe **3** maximizes tumor visualization and improves resection outcomes. Furthermore, unbound probe **3** and its enzymatic product ICG (as ICG-protein complexes) are rapidly excreted via the hepatobiliary system, preventing undesired accumulation *in vivo*. In contrast, non-clinical probes face major limitations, including passive accumulation for targeting, insufficient sensitivity for low-grade gliomas, and static fluorescence without real-time feedback on tumor metabolism or residual activity, leaving micro-residual tumors undetected in a significant fraction of GBM cases.



With advancing development, the field is moving toward conjugating targeted ligands or antibodies with NIR fluorophores, as exemplified by probe **4**.⁵⁴ Structurally, the fully humanized panitumumab moiety specifically binds to the extracellular domain III of epidermal growth factor receptor (EGFR). It blocks ligand-induced receptor dimerization and subsequent downstream signaling. Meanwhile, conjugation with an 800 nm NIR fluorophore enables around 10 mm deep tissue penetration and weakens autofluorescence. This design achieves accurate intraoperative localization of deep-seated high-grade gliomas (Fig. 1C b). These structure-determined properties translate into satisfying clinical performance: probe **4** achieves 95% sensitivity and 96% specificity, representing a 45% improvement over cetuximab-IRDye800CW. Besides, its fully humanized antibody design minimizes immunogenicity risk (adverse event rate <0.5%) and lowers the detection threshold 3-fold compared with cetuximab-IRDye800CW. Additionally, *in vivo*, probe **4** is proteolytically degraded into peptide fragments, amino acids, and the IRDye800CW fluorophore, all of which are rapidly metabolized via the hepatobiliary route. Leveraging these properties, probe **4** balances safety and efficacy while optimizing tumor visualization. By demonstrating both high clinical performance and safety, probe **4** not only validates the feasibility of human application but also provides a roadmap for guiding the design and translation of non-clinical probes toward clinical use.

Table 1 Summary of the fluorescent probes currently used in clinical practice, including their functions and clinical effects.

Disease	Probe	Original name	$\lambda_{ex}/\lambda_{em}$ (nm)	Probe function and clinical effects	Refs.
Nervous system					
Glioma	1	5-ALA	407/635	Uptaken by PEPT1/2 in tumor cells and converted to PpIX; red tumor tissue in surgical cavity; complete resection of tumor.	59, 61
Glioma	3	BLZ-100	785/822	Targets CIC-3 in glioma cells; NIR fluorescence & in situ tumor imaging.	64
Glioma	4	Panitumumab-IRDye800CW	789/800	Crosses BBB, targets EGFR in gliomas; strong NIR fluorescence in tumor core and infiltrative margin.	54
Circulatory system					
Angiosarcoma	5	Ce6-PVP	400/665	Generates singlet oxygen under light to kill tumor cells; the lesion had clear fluorescence compared with normal skin.	65
Atherosclerosis	6	ICG	785/810	Localizes to macrophage, lipid, and exit regions of the plaque; fluorescence indicates endothelial damage.	66
HNSCC	7	Cetuximab-IRDye800CW	778/795	Targets tumor EGFR; high fluorescence in tumor-positive lymph nodes.	67
Respiratory system					
NSCLC	8	OTL38	776/793	Targets tumor FR- α with deep tissue penetration; accurately identifies normal and subcentimeter pulmonary nodules.	68
Lung nodules	6	ICG	785/810	ICG emulsion accumulates around pulmonary nodules; no intraoperative fluorescence diffusion.	69
NSCLC	9	VGT-309	785/820	Fluorescence activated by tumor cathepsins; strong in situ fluorescence in targeted tumors.	70
NSCLC	8; 10	OTL38; Folate-FITC	776/793; 490/520	Longer wavelength fluorescence enables more efficient tumor detection; detects small, invisible tumors.	71
Digestive system					
OSCC	11	Hypericin	450/590	Photosensitive red fluorescent probe; fluorescence intensity increases from normal tissue to carcinoma.	72
HNSCC	7	Cetuximab-IRDye800CW	778/795	High sensitivity & specificity for HNSCC tumors; clear tumor-normal boundary.	73
HNSCC	4	Panitumumab-IRDye800CW	789/800	High tissue penetration NIR probe; visualizes deep-seated tumors.	74
OSCC	12	PARPi-FL	507/525	Targets tumor PARP1, inhibits DNA repair; large lesions show strong fluorescence.	75
OSCC	13	cMBP-ICG	789/803	Targets tumor c-MET receptor; no positive margins in surgical cavity.	76
Gastric cancer	6	ICG	785/810	NIR fluorescence in sentinel lymph nodes; increased lymph node dissection.	77, 78
CRC	14	HAL	407/635	Converts to photosensitive PpIX in tumor cells; selective red fluorescence in rectal adenomas.	79
CRC	15	GE-137	640/680	Targets c-Met in polyps; hyperplastic & serrated polyps show strong fluorescence.	80
CRC	16	cRGD-ZW800-1	785/800	Targets tumor integrins; intraoperative imaging shows intestinal wall tumor fluorescence & enhanced ureteral fluorescence.	81
HCC	6	ICG	785/810	NIR- I / II dual-mode probe; homogeneous fluorescence in well-differentiated HCC.	82, 83
Reproductive system					



Breast cancer	6	ICG	785/810	Micro-dose fluorophore enables non-invasive SLN detection; shorter surgery time; pre-mixed HSA-ICG shows comparable fluorescence to free ICG; fluorescent lymphatics visible in forearm and incision.	84-87
Breast cancer	17	Bevacizumab-800CW	780/800	Targets tumor VEGF-A, inhibits angiogenesis; selective tumor fluorescence in surgical cavity.	88
Ovarian cancer	10	Folate-FITC	490/520	Targets ovarian cancer FR- α ; tumor-specific fluorescence in abdominal cavity.	89
Ovarian cancer	8	OTL38	776/793	High TBR and long duration; sustained strong tumor fluorescence.	90
Prostate cancer	18	ICG- ^{99m} Tc-NanoCol	785/810	Radio-fluorescent dual-modal probe; NIR laparoscopy identifies SLNs with low ^{99m} Tc-NanoCol background.	91
Urinary system					
RCC	10	Folate-FITC	490/520	Completely resected renal mass with clear tumor fluorescence.	92
CRMs	6	ICG	785/810	NIR-II fluorescence in renal parenchyma and tumor vessels.	93
Bladder cancer	19	PLSWT7-DMI	774/789	Targets tumor CD44v6; tumor-specific fluorescence in NMIBC; no signal in nonneoplastic lesions.	94
Bladder cancer	20; 21	Fotoran e6; Fotoditazin	660/671; 660/671	No phototoxicity or bladder contracture after irradiation.	95
Ureteral injury	22	Methylene blue	670/700	NIR microprobe; clearly visualizes ureters with fluorescence lasting ≥ 1 h.	96

View Article Online
DOI: 10.1039/D6SC02520J

2.2 Clinical probes for circulatory system

The human circulatory system facilitates cancer metastasis through blood and lymphatic routes, yet its vessels remain vulnerable to diseases such as angiosarcoma, atherosclerosis, and tumor-positive lymph nodes.⁹⁷⁻⁹⁹ Conventional imaging (MRI, CT, and US) often fails to precisely localize metastatic lesions, whereas fluorescent probes have emerged as powerful tools for real-time diagnosis and guided resection, as summarized in Fig. 2A, which illustrates their clinical applications and research progress.

2.2.1 Clinical probes for blood vessels

Simple photosensitizers like chlorin e6 (Ce6) and 5-aminolevulinic acid (5-ALA) suffer from weak tumor-targeting.^{100, 101} To address this limitation, one approach is to modify photosensitizers, as demonstrated by the development of photosensitizer **5**.⁶⁵ This probe is structurally defined by the conjugation of Ce6 with polyvinylpyrrolidone (PVP) (Fig. 2B), which determines its selective accumulation in tumors by exploiting microenvironment traits such as high metabolic activity. Functionally, the hydrophilic PVP moiety prevents Ce6 aggregation, enhancing cellular uptake and therapeutic efficacy. Upon 400 nm light excitation, photosensitizer **5** emits 665 nm red fluorescence (Fig. 2C c) and produces cytotoxic singlet oxygen (¹O₂) for photodynamic therapy. These structure-driven properties translate into clinical advantages: in angiosarcoma patients, photosensitizer **5** achieves superior tumor specificity (83% vs 73% for Ce6), allowing clear differentiation between tumor and normal tissue.

Compared to the advantages of probe **5**, we can see that non-clinical probes still require several improvements before they can be applied in the clinical treatment of angiosarcoma: 1) Overcoming passive targeting that relies on the enhanced permeability and retention (EPR) effect, as tumor heterogeneity leads to uneven accumulation, with insufficient uptake in about 30% of cases. 2) Structural design: hydrophobic moieties may cause intracellular aggregation and fluorescence quenching, while certain double bonds in the conjugated linker are prone to photochemical instability. 3) Metabolic completeness: clinical use requires probes not to persist in normal tissues, which could cause photosensitivity contraindications within 48 hours. For instance, probe **5** is rapidly eliminated mainly via the hepatobiliary pathway, with negligible residual retention *in vivo* postoperatively. We recommend that this be addressed by using environment-specific release mechanisms, such as selective Ce6 release in acidic or enzyme-rich microenvironments, or by incorporating degradable linkers to ensure automatic deactivation of fluorescence and cytotoxicity within 24 hours post-surgery. Additionally, some structural differences and challenges between clinical and non-clinical photosensitizers are summarized in Table 2.



Apart from angiosarcoma, carotid atherosclerosis is another major vascular disease.^{102, 103} The commonly used methods for detecting atherosclerotic plaques can only observe their location or morphology, but cannot identify high-risk biological characteristics.¹⁰⁴ However, fluorescent probe **6** has shown success in its first clinical study for atherosclerosis patients.⁶⁶ Its mechanism of targeting plaques is based on such a design strategy: 1) It binds non-covalently to albumin and lipoprotein, accumulating in the damaged intima. Such protein complexes passively accumulate in diseased tissues via the EPR effect; 2) it localizes in lipid, macrophage, and hemorrhage areas due to uptake by diseased tissues; 3) NIRF-OCT imaging reveals plaque location, shape, and high-risk features

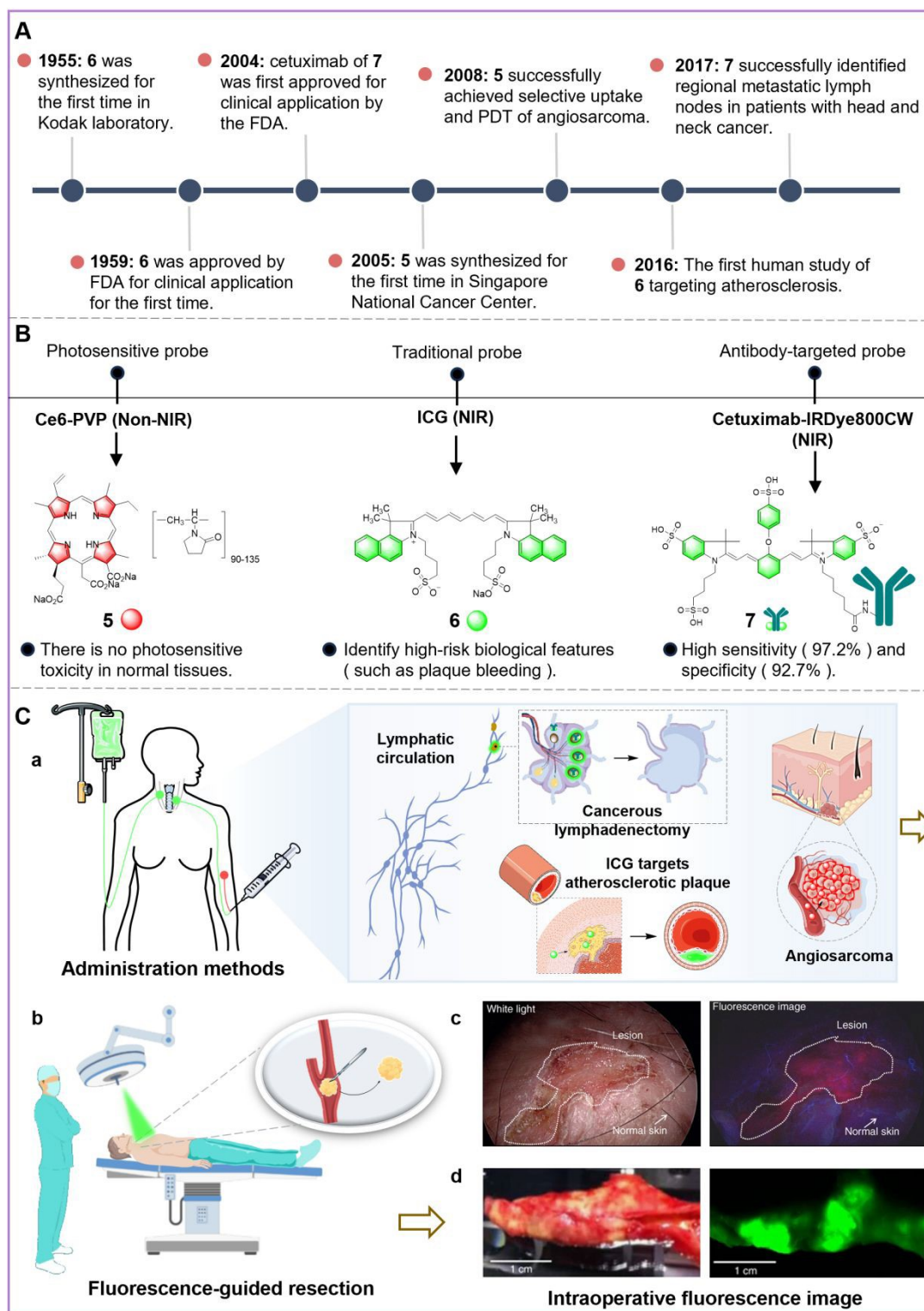


Fig. 2 (A) The timeline of research progress of fluorescent probes in the circulatory system. (B) The chemical structures, categories, and clinical efficacies of the probes. (C) Administration methods, *in vivo* fluorescence mechanisms, intraoperative fluorescence-guided resection methods, and clinical fluorescence images during surgery of the probes. (C c) Reproduced from ref. 65 with permission from Elsevier Ltd, copyright 2008. (C d) Reproduced from ref. 105 with permission from Springer Nature, copyright 2017.

(Fig. 2C b). When comparing probe **6** to non-clinical probes, we find it offers several advantages: 1) High detection success rate: probe **6** achieves a 100% detection rate for plaques in clinical use. 2) Distinct signal characteristics: its strong green fluorescence allows clear lesion identification by physicians (Fig. 2C d). 3) Identification of a new target: probe **6** targets intraplaque hemorrhage, which was not seen in previous animal studies, thus overcoming prior research limitations focused on macrophages and lipids. 4) Capability to assess plaque risk and severity: combined with NIRF-OCT imaging, probe **6** reveals plaque location, shape, and high-risk features like hemorrhage, aiding in severity and risk assessment. In addition, probe **6** is rapidly cleared via the hepatobiliary pathway. We think, these advantages, driven by probe **6**'s structure and strategy set the "entry threshold" for clinical use and minimize research risks.

2.2.2 Clinical probes for lymph nodes

Lymph is an important way for the metastasis of tumor cells except blood vessels.¹⁰⁶ However, white-light surgery often fails to completely resect these lymph nodes, which is attributed to the lack of visual feedback and targeting of tumors.¹⁰⁷ Residual tumor-positive lymph nodes will increase the probability of cancer recurrence and metastasis. In order to maximally resect these lymph nodes, a method of lymph node visualization is necessary. With advances in lymphatic fluorescence imaging, probe **7** has shown initial success in lymph node detection in head and neck cancer (HNC).⁶⁷ The design strategy of probe **7**, which combines cetuximab, an EGFR-targeted drug, with the NIR fluorophore IRDye800CW, enables its successful application in HNC (Fig. 2B): 1) high EGFR expression, facilitating tumor and tumor-positive lymph node targeting; 2) cetuximab binding to EGFR domain III, blocking downstream signaling; and 3) fluorescence emission from lymph nodes upon probe localization in cancer cells (Fig. 2C a). Based on these features, probe **7** provided high sensitivity (97.2%) and specificity (92.7%) for identifying positive lymph nodes in HNC patients. Strategically, deeper sectioning of fluorescent "false positives" revealed hidden cancer cells, thereby detecting metastases missed by standard methods. As such, this strategy reduces unnecessary lymph node resections and improves patient survival, demonstrating the crucial role of both structure and strategy in advancing clinical outcomes.

Drawing upon the clinical advantages of this probe, we propose the following insights to guide the development of future clinical probes. 1) Achieving ultra-high sensitivity and specificity is crucial. We recommend that even probe **7** require further optimization, as these metrics are key to differentiating benign from malignant lesions and identifying lymphoma subtypes. 2) Multitarget and multicolor detection are essential. After all, probes with multi-color labeling can enable simultaneous detection of multiple targets, avoiding signal overlap and photobleaching, which is critical for diagnosing lymphomas with complex genetic alterations. 3) Chemical strategies to enhance stability and standardization are vital; modifications like dye rigidification, hydrophilic tuning, and charge regulation can significantly improve photostability, ensuring signal persistence during prolonged observation. 4) Optimizing pharmacokinetics and clearance profiles is necessary; adjusting probe hydrodynamic radius can maximize tumor-to-background contrast within the optimal imaging window and ensure metabolic degradation, thus reducing long-term toxicity. As exemplified by probe **7**, the extremely low residual toxicity *in vivo* is attributed to its rapid hepatic metabolism and subsequent biliary excretion.

2.3 Clinical probes in respiratory system

The respiratory system serves for absorbing oxygen and releasing carbon dioxide in the human body, which includes the respiratory tract (nose, pharynx, larynx and trachea, etc.) and the lung.^{108, 109} To discuss the probes for lung cancer, we summarized the recent clinical research in patients (Fig. 3A).



2.3.1 Clinical probes for lung

View Article Online
DOI: 10.1039/D6SC02520J

For non-small cell lung cancer (NSCLC),¹¹⁰ standard white-light surgery for NSCLC often misses small nodules, leading to recurrence.¹¹¹ Fluorescent probe **8** was applied to NSCLC patients and confirmed the feasibility of FGS for the treatment of NSCLC.⁶⁸ **8** is synthesized from folate combined with an NIR fluorophore (Fig. 3B), and its design strategy is based on the following principles: 1) Since most NSCLCs overexpress folate receptor- α (FR- α), **8** targets tumors expressing FR- α (Fig. 3C a) through high-affinity folate binding via endocytosis. 2) The lung nodules containing **8** emit red fluorescence (around 800 nm) (Fig. 3C b). Based on these structural features, probe **8** demonstrated excellent clinical efficacy in NSCLC patients, achieving a 100% identification rate and successfully localizing sub-centimeter lesions. Its superior targeting and NIR properties, with low autofluorescence and deep tissue penetration, provide a distinct advantage over conventional probes like ICG, enabling the detection of small nodules often missed during standard surgery. Furthermore, it exhibits negligible *in vivo* retention, being rapidly cleared via the kidneys and excreted in urine.

Table 2 Comparison of clinical and non-clinical photosensitizers.

Probe	Disease	Advantages / limitations	Refs.
Clinical probes			
Ce6-PVP	Angiosarcoma	High uptake rate; fast metabolic rate; non-phototoxicity to normal tissues.	65
Hypericin	Oral cancer	Clear fluorescence tumor edge; almost no blood circulation; no systemic toxicity.	72
Structural advantages from clinical probes			
<ul style="list-style-type: none"> ● The rigid plane provides high molecular stability. ● The planar structure prevents free rotation and vibration of the molecular structure. ● Low non-radiative transitions. 			
Non-clinical probes			
TPA-DCR	Breast cancer	Complex preparation methods; limitations in treating deep-seated tumors.	112
⁸⁹ Zr-PHZ-BrCyE	Liver cancer	Radiation exposure risk; pH-responsive micelles have the possibility of non-specific uptake (inflammatory tissue).	113
Chemical challenges from non-clinical probes			
<ul style="list-style-type: none"> ● Hydrophobic structures may cause the probe to aggregate and quench within cells. ● The cis-trans isomerization of the molecule disrupts its rigid planar structure. ● The double bond in the conjugated bridge exhibits photochemical instability and readily breaks under oxidative conditions. ● The small conjugated range results in a low fluorescence quantum yield. 			

As we can see, this clinical application reveals that the respiratory system, particularly the lungs, possesses unique anatomical and physiological characteristics, imposing specific demands on fluorescent probes in clinical settings. 1) There is an urgent need for probes with exceptional tissue penetration depth to enable non-invasive or minimally invasive imaging of lung parenchyma or mediastinal lymph nodes. We believe integrating X-ray or ultra-active functional groups with probes may offer a viable solution. 2) Overcoming strong background interference and autofluorescence is critical, as lung tissue contains collagen fibers, elastin, and inhaled particulates that generate nonspecific signals. Thus, probes must exhibit ultrahigh signal-to-noise ratios to distinguish pathological signals from complex backgrounds. 3) Probes administered systemically must traverse the 'air-blood barrier' to reach lung parenchyma. We think designing small-molecule probes or conjugating cell-penetrating peptides (e.g., Trans-activator of transcription peptide (TAT), Octa-arginine (R8)) could significantly enhance their efficiency in crossing physiological barriers and entering lung tissue from circulation.

While for the imaging of lung nodules, even the mature probe **6** has limitations in penetration depth and diffusion.¹¹⁴ Optimizing its state or changing its dosage form can resolve these limitations.^{115, 116} The first probe used



in human to prevent the diffusion of **6** gives us a new method: a fluorescent iodized emulsion (water: oil = 1:6) and emulsified by **6** and ethiodized oil.⁶⁹ The design principle of this method involves: 1) To locate tumors accurately, physicians use fluoroscopic CT to identify lung nodules before surgery and then inject this emulsion at the nodule margins.¹¹⁷ As a result, **6** binds with human albumin after injection, enabling passive targeting and accumulation in

View Article Online
DOI: 10.1039/D6SC02520J

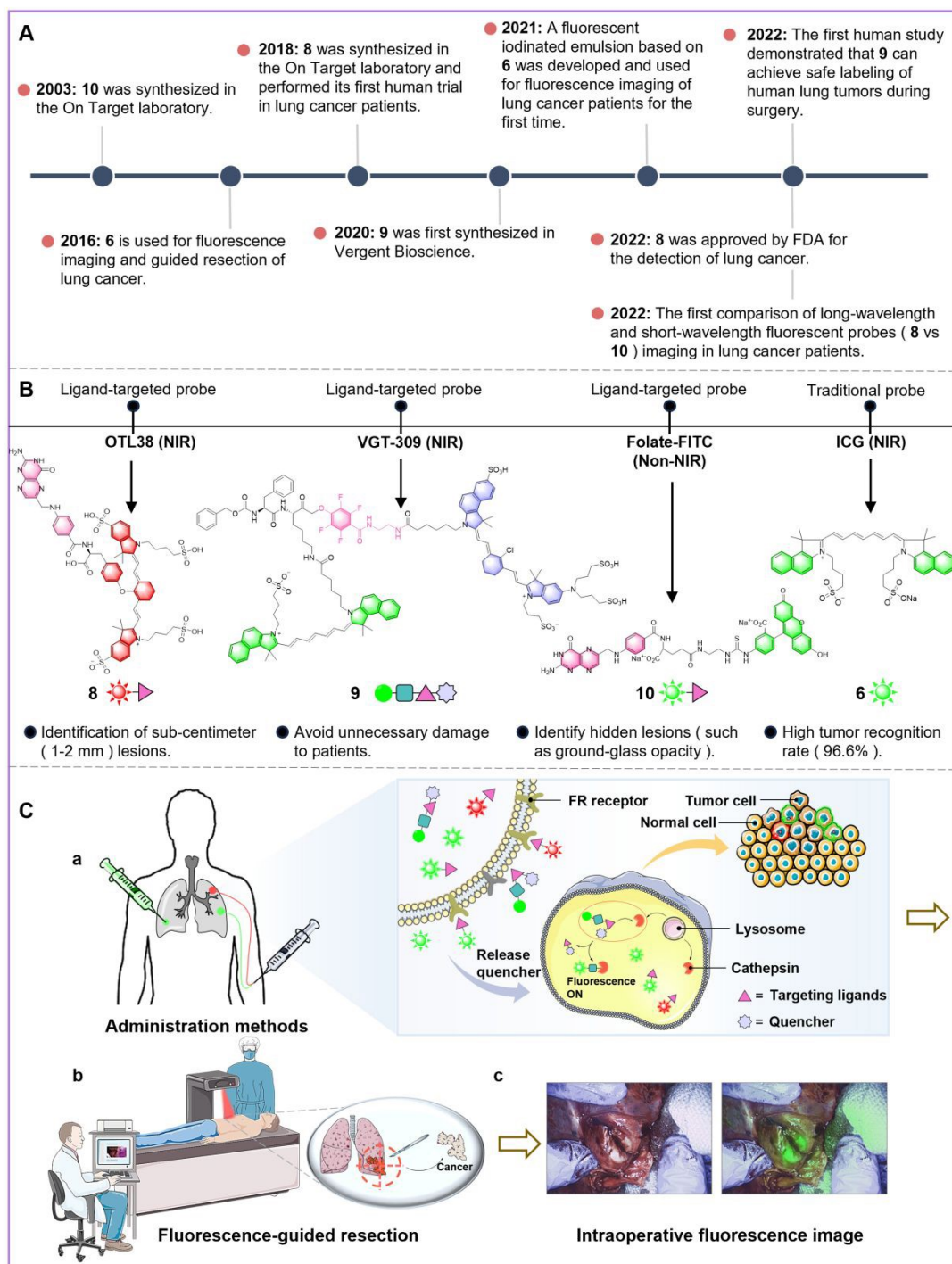
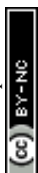


Fig. 3 (A) The timeline of research progress of fluorescent probes in the respiratory system. (B) The chemical structures, categories, and clinical efficacies of the probes. (C) Administration methods, *in vivo* fluorescence mechanisms, intraoperative fluorescence-guided resection methods, and clinical fluorescence images during surgery of the probes. (C c) Reproduced from ref. 118 with permission from American Medical Association, copyright 2023.

the nodules. In addition to the EPR effect, this accumulation is also attributed to the endocytosis of albumin-bound



complexes mediated by SPARC (secreted protein acidic and rich in cysteine), an albumin-binding receptor overexpressed by tumor cells;¹¹⁹ 2) The water-in-oil emulsion prevents diffusion of probe **6**, allowing it to accumulate maximally in the nodules. This in turn, increases fluorescence intensity, which further enhances the detection depth of nodules. The emulsion shows strong clinical potential by forming stable water-in-oil droplets that prevent diffusion and quenching of compound **6**, maintaining 6-day stability, achieving 66.6% lung nodule detection, and extending penetration to 25 mm (vs. 10 mm for compound **6**) (Fig. 3C c). However, the current method of mixing iodide oil and compound **6** lacks consistency, highlighting the need for more reliable carrier development.

From this clinical application, we can find that the water-in-oil emulsion strategy illustrates how physical encapsulation can improve both probe stability and clinical utility, while passive targeting via human albumin binding boosts nodule accumulation. This integrated approach underscores three actionable principles: 1) Dual-functional carrier design that combines probes with approved agents for imaging or therapeutic synergy. Such design accelerates clinical application, enhances diagnostic precision, reduces side effects, and enables personalized treatment. 2) Endogenous protein-mediated targeting to enhance tissue retention. We believe it would improve targeting accuracy, prolong treatment effects, and offer broad clinical applications with natural biodegradability. 3) Multimodal guidance, using both CT and fluorescence, for precise delivery to deep lesions, which could be an adaptable framework for other probe systems that require depth and specificity.

Table 3 Comparison of clinical and non-clinical probes in emission wavelength.

Type	Probe	Disease	Advantages / limitations	Refs.
Clinical probes				
NIR probes	Bevacizuma b-800CW	Breast cancer	High tumor background ratio; clear tumor positive margin; deep tissue penetration.	88
	PLSWT7-DMI	Bladder cancer	Detection of small and flat lesions; accurate tumor localization; clear intraoperative fluorescence.	94
Non-NIR probes	Folate-FITC	Ovarian cancer	High tumor recognition rate; stable fluorescence signal; identify metastatic lesions.	89
	GE-137	Colon cancer	High tumor specificity; assisted minimally invasive surgery.	80
Structural advantages from clinical probes				
<ul style="list-style-type: none"> ● Heptamethine conjugated bridge provides a large conjugated system. ● Small HOMO-LUMO energy gap. ● Highly symmetrical structures minimize energy loss. ● The π electrons are highly delocalized within the conjugated system. 				
Non-clinical probes				
NIR probes	Tg-RGD	Breast cancer	GSH-responsive probes may be affected by liver and inflammatory tissues; low blood GSH may shorten probe half-life.	120
	DCM- β gal	Colon cancer	May activate in other tissues (aging cells); natural β -gal substrates may compete with probe for enzyme binding.	121
Non-NIR probes	HPL-1	Liver cancer	May be interfered by low-pH normal tissues; possible competitive binding with endogenous galactose.	122
	BO-biotin	Liver cancer	Endogenous biotin interference; may be non-specific accumulation.	123
Chemical challenges from non-clinical probes				
<ul style="list-style-type: none"> ● The narrow conjugation range and the accompanying high non-radiative transitions result in a low fluorescence quantum yield. ● The targeting groups are interfered with by endogenous substances in the body. ● The double bonds in the conjugated bridge exhibit photochemical instability and are prone to oxidative cleavage within the body. ● Risk of <i>in vivo</i> metabolite toxicity posed by risk groups. 				

For FGS to treat lung cancer, if we have a “smart” probe, we can achieve high tumor targeting, deep tissue penetration and favorable biosafety.¹²⁴ A clinical study that uses a quenched activity-based probe (qABP) **9** to identify the tumors of patients with lung cancer is reported.⁷⁰ Mechanistically, with the overexpression of cathepsins in many organs, **9** can covalently combine with cathepsins of tumor cells by its phenoxymethyl ketone electrophile; the quencher QC-1 will be broken after **9** is combined with cathepsins, and then the fluorescence characteristic of **9** (from fluorophore ICG) will be opened (Fig. 3C a). Probe **9** demonstrates high clinical value in lung cancer surgery,



achieving tumor-background ratio >2.0 and enabling visualization of subpleural tumors (~17 mm depth) during minimally invasive wedge resection, thereby reducing surgical trauma and improving outcomes. In tumor cells, enzymatic cleavage of its targeting peptide releases the ICG fluorophore, which is ultimately eliminated via the hepatobiliary pathway. Moreover, the human trials confirm its feasibility and safety. Notably, since cathepsins are expressed across multiple tumor types (kidney, thymus, etc.), probe **9**'s application could extend to other cancers.¹²⁵ Similarly, **8** and **10** are also the “smart” probes for the lung tumor resection (Fig. 3B). Both probes target FR- α , which is overexpressed in lung tumor cells. After intravenous injection, they enter tumor cells, allowing physicians to use different light wavelengths for fluorescence imaging. Preoperatively, probe **8** shows a higher detection rate than probe **10** (75.4% vs. 23.9%) and locates tumors nearly three times more effectively. Additionally, probe **8** can detect tumors at greater depths (18 mm vs. 3 mm), while probe **10** is limited to surface tumors. Based on this, we conducted a comparative analysis (Table 3) between these probes with non-clinical probes and analyzed the structural advantages of clinical probes (Fig. 4), where we can see the gap between the two mainly lies in low *in vivo* fluorescence efficiency, poor stability, and potential toxicity: 1) Low fluorescence quantum yield; 2) Targeting groups are interfered with by endogenous substances; 3) Conjugated double bonds are photochemically unstable and prone to oxidative cleavage; 4) Certain structural groups may generate toxic metabolites. Nevertheless, folate released from the degradation of clinical probes such as **8** and **10** poses no biosafety risks, and their fluorophores (S0456 and FTIC dyes) are rapidly excreted renally. By addressing these gaps, new probes can be developed with better fluorescence efficiency, stability, selectivity, and safety, paving the way for effective clinical applications.

2.4 Clinical probes for digestive system

Cancers in the digestive system include oral cancer, gastric cancer, and colorectal cancer.¹²⁷ For the resection of digestive system cancers, fluorescent probes give them great hope. Given their diverse clinical applications, we summarize the structural characteristics of these probes as follows: 1) The balance between the positive quaternary ammonium and negative sulfonate charges within the probe molecule minimizes non-specific protein binding. 2) The connection bond between the fluorescent group and the targeting group is of optimal length, reducing steric hindrance and minimizing interference. 3) A rigid plane, such as Hypericin, prevents intramolecular rotation and vibration, thus enhancing the fluorescence stability of the molecule. 4) Lipid modification, such as HAL, increases the probe's fat solubility, facilitating its entry into tumor cells. 5) The large conjugated system provided by the heptamethine bridge improves deep tissue penetration, enabling detection of small or flat lesions in deeper organs such as the colon, stomach, and liver. The specific applications and characteristics in each sub-organ are detailed in the discussion below.

2.4.1 Clinical probes for upper digestive tract

2.4.1.1 Oral cavity

The main treatment of oral squamous cell carcinoma (OSCC) is surgical resection combined with radiotherapy and chemotherapy, and pathology biopsy is also required among them.^{128, 129} Unfortunately, even with a white-light endoscope, complete tumor resection is challenging because physicians lack sufficient visual and tactile feedback, thus leading to repeated surgery and increasing the frequency of pathological biopsy.¹³⁰ Many fluorescent probes have been applied to intraoperative imaging of digestive system tumors (Fig. 5A). Among them, a clinical study with probe **11** to detect and resect tumors of OSCC patients provides us with a guidance.⁷² With a design of subcellular accumulation in the endoplasmic reticulum, lysosomes, Golgi apparatus, and mitochondria, this photosensitizing probe enables OSCC tumor localization via a 30-minute oral rinse and intraoperative fluorescence guidance (Fig. 5C b). The clinical efficacy of probe **11** for OSCC detection arises from its unique chemical properties: its extended π -conjugation system generates strong red fluorescence (~590 nm), which provides superior tissue



contrast compared to white light endoscopy, with over 90% sensitivity and specificity for OSCC localization. Additionally, the enhanced R/B intensity ratio helps to distinguish normal, hyperplastic, and cancerous tissues. Moreover, the phenolic hydroxyl groups present opportunities for structural optimization, including conjugation with OSCC-targeting ligands (e.g., EGFR antibodies) or PEGylation, which can further enhance tumor selectivity. Unused probe **11** is rapidly eliminated via the hepatobiliary system. Therefore, we have outlined several structural optimizations and design strategies in BOX 1 to improve specificity for OSCC.

As a comparative analysis, probes **4** and **7** are successfully applied in head and neck squamous cell carcinoma (HNSCC: oral part).^{73, 74} The results demonstrate they have superior clinical performance over probe **11** through 3

View Article Online
DOI: 10.1039/D6SC02520J



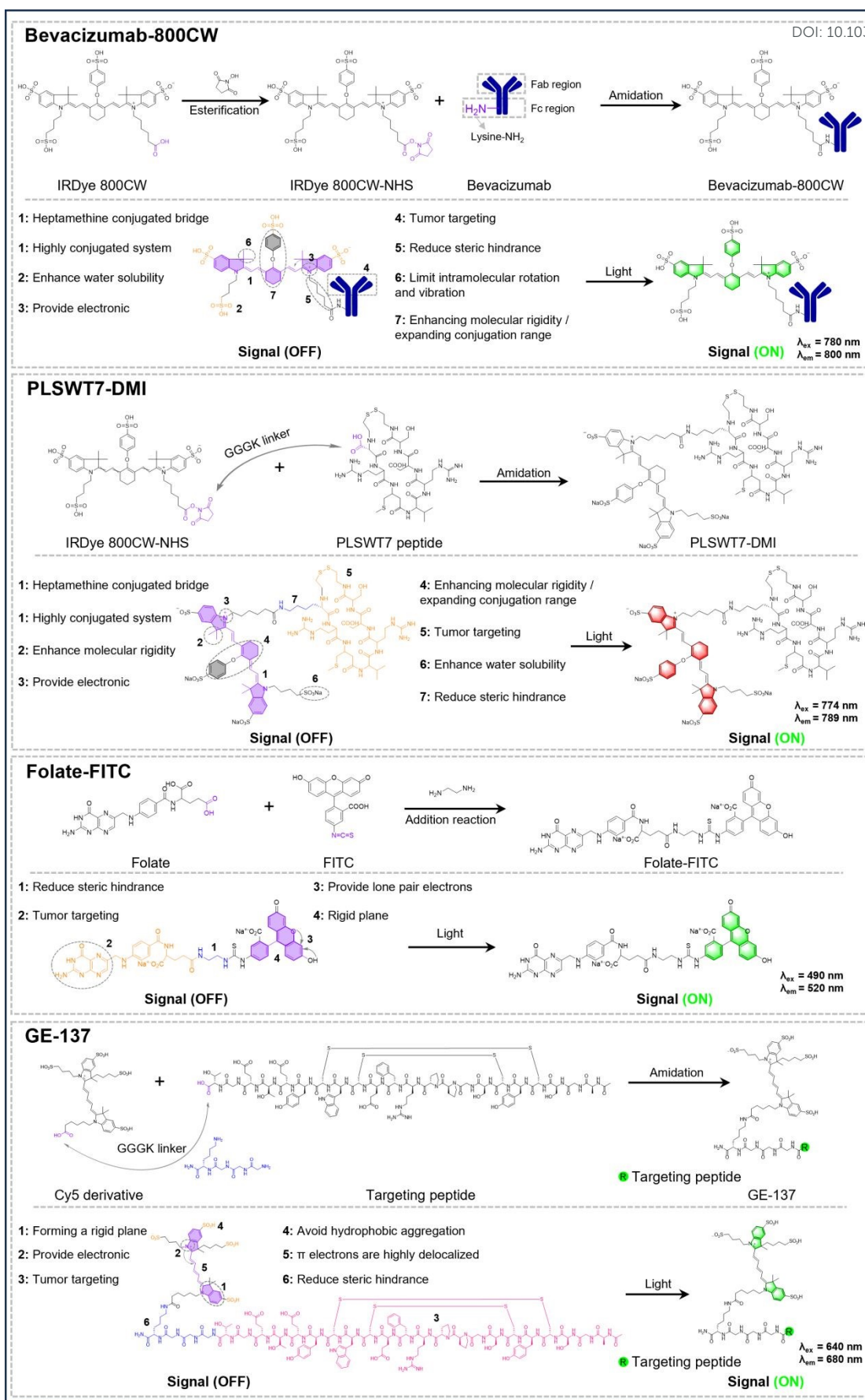


Fig. 4 Synthetic methods and structural analysis of bevacizumab-800CW (Probe 17; IRDye 800CW fluorophore), PLSWT7-DMI (Probe 19; IRDye 800CW fluorophore), folate-FITC (Probe 10; FITC fluorophore) and GE-137 (Probe 15; Cy5 derivative fluorophore).



key advancements: 1) Targeted specificity via EGFR antibodies (cetuximab/panitumumab) achieving >80% sensitivity/specificity, eliminating non-specific uptake issues; 2) Enhanced imaging with NIR capabilities enabling 10 mm tissue penetration and 3-fold tumor-to-normal fluorescence contrast for precise margin delineation, especially for lesions within a 0-5 mm depth range; 3) Optimized safety with panitumumab-compatible structures, about 8-fold higher EGFR affinity while maintaining low toxicity; however, shallow penetration remains a shared limitation requiring future wavelength optimization.

Actually, the development of “smart” probes for oral cancer has never stopped. Probe **12**, a Poly(ADP-ribose) polymerase 1 (PARP1)-targeting probe combines olaparib's inhibitor scaffold with BODIPY-FL (507 nm emission), with structural optimization achieved via cyclopropane substitution (Fig. 5B), and has entered OSCC clinical trials.⁷⁵ Its fluorescence mechanism is determined by its dual-component structure: 1) The olaparib-derived moiety specifically binds the C-terminal catalytic domain (CAT) of overexpressed PARP1 in tumor cell nuclei (due to defective DNA repair), inhibiting single-strand break repair and inducing BRCA-mutated tumor cell death via synthetic lethality; 2) The covalently linked BODIPY-FL fluorophore (507 nm) emits green fluorescence for real-time tumor visualization, enabled by its 11.6-fold higher tumor uptake (45.14% vs 3.89%) compared to normal cells (Fig. 5C c). While effective for margin delineation, BODIPY-FL's short wavelength limits penetration depth, necessitating future optimization. Taking the advantages of tumor overexpression of cellular-mesenchymal epithelial transition factor (c-Met) in OSCC cells, probe **13** was developed as a covalent conjugate of water-soluble small molecules and ICG (Fig. 5B).⁷⁶ Its tumor-targeting capability stems from its c-Met binding peptide (cMBP) structure, which specifically binds to IPT3/4 domains of c-Met receptors, inhibiting receptor dimerization and downstream signaling activation (Fig. 5C a). This molecular design enables deep-tissue tumor detection with high sensitivity, capable of identifying both small deep-seated tumors and precancerous hyperplasia, while offering rapid and safe surgical application.

Based on the clinical application of the aforementioned probes in humans, we believe that non-clinical probes should be improved to meet the requirements of oral diseases: 1) Oral mucosa requires probes with mucus-penetrating capability. We think it can be achieved through polyethylene glycol (PEG) modification or cell-penetrating peptide (CPP) conjugation. 2) Probes need to be stable against enzymatic degradation in saliva. This can be accomplished by using D-amino acids or cyclic structures. 3) Probes should rapidly target and bind, ideally within 30 minutes, which suits the oral microenvironment. Moreover, unbound probes should be rapidly eliminated via the hepatobiliary system like probes **12** and **13** to avoid nonspecific accumulation *in vivo*. 4) When superficial and deep lesions coexist, a balance between penetration depth and fluorescence resolution must be achieved.

2.4.1.2 Stomach

The radical surgery of gastric cancer includes complete resection of tumors and lymph nodes.¹³¹ However, the small surgical cavity in laparoscopic radical gastrectomy (LRG) consistently results in poor visual and tactile feedback for surgeons, which further necessitates reliance solely on experiential judgment.¹³² To evaluate the feasibility and safety of utilizing FGS to augment LRG, a clinical study involving **6** provided satisfactory results.⁷⁸

The clinical efficacy of fluorophore **6** in gastric cancer lymph node resection results from its albumin-binding design: 1) The submucosal injection (proximal/distal/lateral tumor sites) uses the probe's tissue diffusion properties for efficient uptake by tumor-positive lymph nodes via albumin complexation. Uptake of such albumin complexes in tumors is also attributed to the dual effects of the EPR effect and SPARC-mediated internalization; 2) This transport mechanism enables real-time dual visualization of primary tumors and metastatic lymph nodes under laparoscopy (Fig. 5D c), leading to better surgical outcomes, 35 mL less blood loss, 20-30 more lymph nodes



harvested; 3) The fluorophore's optical stability ensures sustained fluorescence, reducing surgical time and complications. In clinical surgery, its utility stems from molecular fluorescence properties: the fluorescence emission (Fig. 5D b) enables real-time lymph node visualization, aiding precise distal gastrectomy (DG) and total gastrectomy (TG) with D2 lymphadenectomy. Moreover,

[View Article Online](#)

[DOI: 10.1039/D6SC02520J](https://doi.org/10.1039/D6SC02520J)



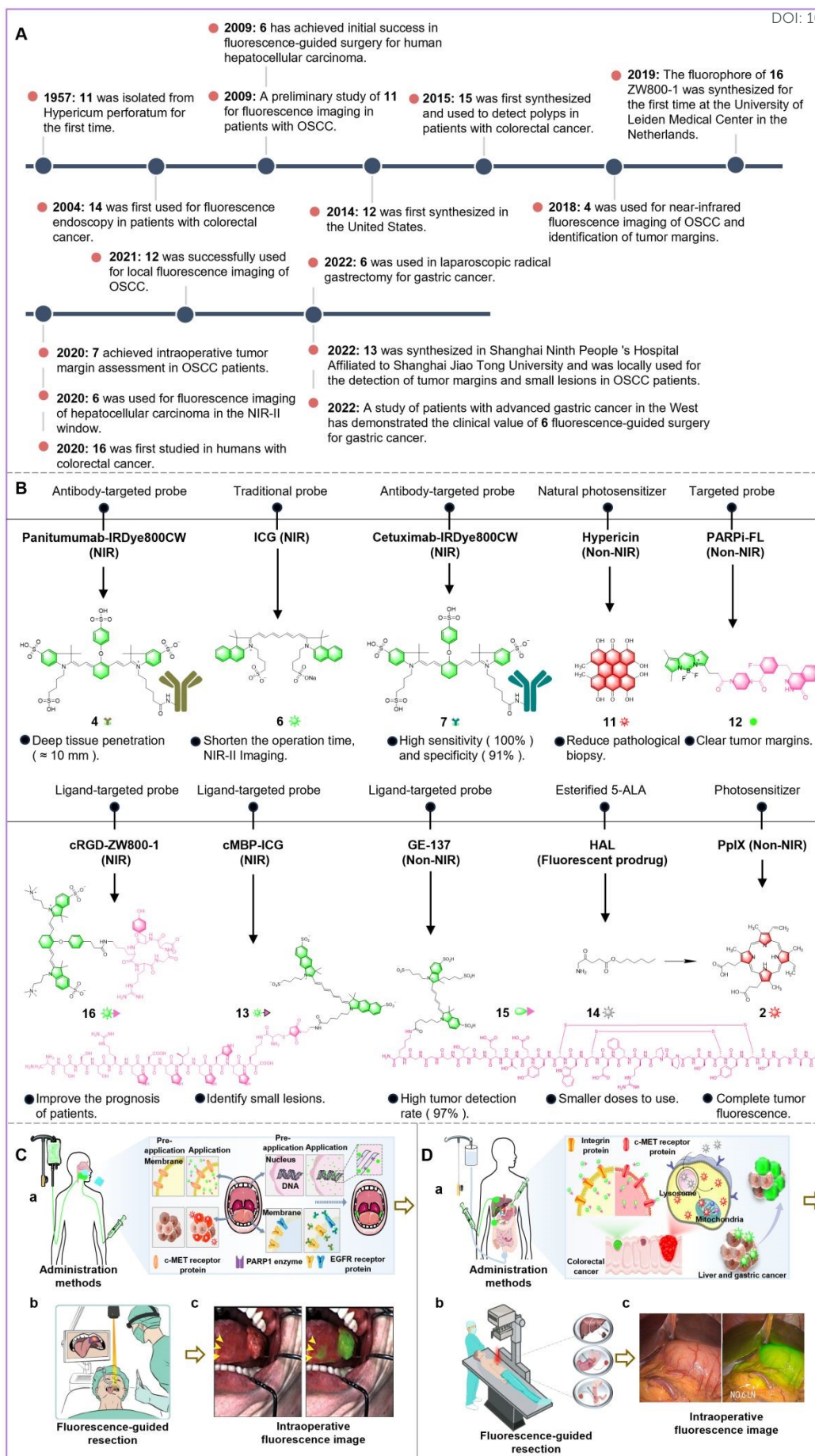


Fig. 5 (A) The timeline of research progress of fluorescent probes in the digestive system. (B) The chemical structures, categories, and clinical efficacies of the probes. (C, D) Administration methods, *in vivo* fluorescence mechanisms, intraoperative fluorescence-guided resection methods, and clinical fluorescence images during surgery of the probes. (C b) Reproduced from ref. 133 with permission from Ivyspring International Publisher, copyright 2025. (C c) Reproduced from ref. 73 with permission from Ivyspring International Publisher, copyright 2020. (D c) Reproduced from ref. 78 with permission from Frontiers Media S.A., copyright 2022.

the persistent signal allows repeated cavity evaluations and iterative lymphadenectomy until complete signal elimination, standardizing surgical quality control beyond traditional lymph node quantification. Clearly, fluorescence probes like this can enhance tumor and lymph node detection, optimize surgical precision, and improve outcomes in gastric cancer surgeries.

2.4.2 Clinical probes for lower digestive tract

2.4.2.1 Colorectum

The common detection methods of colorectal cancer (CRC) include: endoscopy (sigmoid colonoscopy and colonoscopy) and imaging detection (CT, MRI, etc.).^{134, 135} Unfortunately, none of these methods can provide real-time tumor visualization for physicians during surgery. The first human study using probe **14** to detect rectal adenoma confirmed the feasibility of FGS.⁷⁹ **14** is a prodrug obtained by esterification of **1** (Fig. 5B). For tumor localization, **14** and **1** have similar principles.¹³⁶ However, **14** (lipophilic) is obtained from the esterification of carboxyl of **1** (hydrophilic), which makes **14** more easily absorbed and penetrated into tumor cells. The esterase-labile structure of compound **14** enables its tumor-specific hydrolysis to **1**, which is subsequently converted by enzymatic cascades into the photosensitizer **2** (Fig. 5D a), a process amplified by ferrochelatase inhibition-induced accumulation of the fluorescent **2** ($\lambda_{em} \approx 635$ nm). Benefiting from its molecular strategy, the probe has three advantages that make it successful for clinical use: 1) The lipophilic modifications in **14** enhance membrane permeability, allowing quite low doses and shorter infusion while maintaining equal fluorescence intensity; 2) Tumor-selective activation ensures 100% adenoma detection with no off-target phototoxicity, as normal tissues lack the enzymatic milieu for generation of **2**. Unbound probe **14** and its hydrolytic product **1** are rapidly renally excreted in urine; 3) Limited fluorescence in low-grade cancers reflects poor prodrug activation in undifferentiated cells, highlighting the metabolic dependency of this chemical strategy.

In light of these promising results in adenoma detection, researchers have further developed probes to address the challenge of detecting and resecting polyps that are often missed. Fluorescent probe **15** was developed and used for the first time in fluorescence-guided colonoscopy of polyps in patients at high risk for CRC.⁸⁰ The cyclic peptide structure of **15**, composed of a 26-amino acid sequence conjugated with modified sulfo-Cyanine5 (Cy5) dye, confers high c-Met affinity through specific interactions with the extracellular IPT3/IPT4 domains (Fig. 5B), enabling selective tumor targeting in colorectal adenomas and cancers (Fig. 5D a). This design strategy leads to 3 key functional benefits: 1) The peptide-dye conjugate emits bright green fluorescence upon light excitation, achieving 97% detection probability for polyps, including sub-6 mm flat lesions during fluorescence colonoscopy; 2) Unlike locally applied probes, **15**'s systemic applicability stems from its optimized plasma protein non-binding characteristics and safety profile, thereby overcoming colorectal surface coverage limitations; 3) The targeting mechanism parallels **13** by inhibiting c-Met dimerization and downstream signaling, demonstrating structure-activity consistency. Similarly, probe **15** shares a comparable metabolic pathway with **13**, and unincorporated probes are rapidly excreted via the hepatobiliary system.

The standard treatments of CRC include minimally invasive laparoscopic surgery (MIS) and open colectomy.¹³⁷ However, the narrow surgical space of MIS usually provides extremely poor tumor visualization during surgery.¹³⁸ The first-in-human study of probe **16** has been conducted in CRC patients undergoing MIS.⁸¹ The molecular design of probe **16**, combining an integrin-targeting cyclic Arg-Gly-Asp (cRGD) peptide with the zwitterionic fluorophore ZW800-1 (Fig. 5B), reflects a strategic design to achieve tumor selectivity through three key structural features: 1)



The cRGD motif binds integrins (e.g., $\alpha\beta6/\alpha\beta3/\alpha\beta5$) in a cation-dependent manner ($\text{Ca}^{2+}/\text{Mg}^{2+}$), disrupting extracellular ligand interactions and downstream signaling; 2) The zwitterionic design reduces nonspecific uptake, allowing NIR fluorescence with deeper tissue penetration and dual imaging of tumors/lymph nodes, achieving 100% sensitivity and 87% specificity; 3) The zwitterionic scaffold's renal clearance aids in ureter identification during surgery. However, integrin overexpression in non-neoplastic tissues presents diagnostic challenges, requiring clinical differentiation.

BOX 1. The structural descriptions and functions of the target receptors, ligands and antibodies of the probes and the principle of them.

● **EGFR**

Structure and function

EGFR, a 1186-residue transmembrane glycoprotein, comprises an extracellular region (domains I-IV), a transmembrane domain (TM), and an intracellular domain (JM, TK, and C-terminal tail). Its primary ligands include epidermal growth factor (EGF) and transforming growth factor- α (TGF- α); ligand binding triggers downstream signaling cascades, including JAK/STAT (immune regulation), RAS-RAF-MEK (cell proliferation), and PI3K-AKT-mTOR (cell survival).

Differences between cetuximab and panitumumab

Both target domain III of EGFR to inhibit downstream signaling activation. While most binding amino acid residues overlap, they can be distinguished by distinct sites: cetuximab (I467, S468, Q408, H409) and panitumumab (W386, E388, R390, T391).

● **The principle of RGD binding to integrin**

Integrin and RGD

Integrins are transmembrane heterodimers formed by the non-covalent association of α and β subunits. Due to the existence of multiple isoforms of these subunits, integrins are classified into various types (e.g., $\alpha\beta6$, $\alpha\beta3$, $\alpha\beta5$). The tripeptide RGD motif, widely present in extracellular matrix proteins such as fibronectin and laminin, mediates the specific binding to integrins.

Principle

Divalent cations (e.g., Ca^{2+} , Mg^{2+}) support specific binding of fibronectin/laminin RGD motifs to the extracellular domain of integrins. The linkage between integrin intracellular domains and actin cytoskeleton enables bidirectional coupling between the extracellular matrix and intracellular skeleton, facilitating tumor cell adhesion and migration. Cyclic RGD (cRGD) inhibits these processes via integrin binding, and fluorophore-conjugated cRGD enables targeted fluorescence imaging.

● **CD44v6: structure and function**

CD44v6, a major CD44 isoform encoded by its sixth variant exon, is a transmembrane glycoprotein comprising extracellular, transmembrane, and intracellular domains. The extracellular region contains an N-terminal globular domain and a membrane-proximal region, with the N-terminal domain mediating ligand binding to hyaluronic acid (HA). The intracellular domain activates MAPK/ERK and PI3K/Akt signaling, thereby regulating cancer cell growth and metastasis. HA specifically binds the CD44v6 extracellular domain, inducing intracellular domain phosphorylation and downstream signaling activation, which modulates cell growth, metastasis, and apoptosis.

● **The principle of glioma migration**

To infiltrate the narrow extracellular matrix, glioma cells reduce their volume and adopt an elongated or wedge-shaped morphology prior to migration. To maintain the cellular isoelectric point upon shrinkage, intracellular Cl^- and K^+ efflux via chloride channel-3 (ClC-3) and potassium-calcium ion channel (KCa3.1), respectively. This ion efflux activates water channels, promoting water outflow and inducing regulatory volume decrease (RVD), which facilitates glioma cell migration.

● **c-Met: structure and function**

c-Met is a transmembrane protein encoded by the human proto-oncogene, which binds its ligand hepatocyte growth factor (HGF) and activates multiple signaling pathways. Its extracellular region consists of an N-terminal SEMA domain, a cysteine-rich domain, and four IPT domains; the intracellular region includes a juxtamembrane domain (Tyr1003, Ser985), a catalytic domain (Tyr1234, Tyr1235), and a C-terminal multifunctional docking region (Tyr1349, Tyr1356). HGF binds with high affinity to the IPT3/IPT4 domains and low affinity to the SEMA domain of c-Met. Upon HGF binding, c-Met undergoes dimerization and phosphorylation, activating downstream pathways including PI3K/Akt, RAS/MAPK, and STAT3, which regulate cell growth, proliferation, and migration.

● **PARP-1**

Structure and function

PARP-1 comprises an N-terminal DNA-binding domain (DBD), a central auto-modification domain (AD), and a C-terminal catalytic domain (CAT). PARPi-FL inhibits its catalytic activity by binding to the CAT domain. PARP-1 is activated by nicotinamide adenine dinucleotide (NAD^+) and primarily mediates cellular DNA repair.

Synthetic lethality (such as BRCA mutant cells)

BRCA mutation impairs homologous recombination, rendering cancer cells dependent on PARP-1 for DNA repair. Inhibition of PARP-1 abrogates this pathway, inducing irreparable DNA damage and cell death. This dual targeting strategy, termed synthetic lethality, exploits the underlying deficiency to eliminate tumor cells.

● **The function of VEGF and VEGFR**

VEGF

VEGF is a homodimeric protein, and its family comprises VEGF-A, VEGF-B, VEGF-C, VEGF-D, VEGF-E and placental growth factor (PGF). VEGF-A specifically binds to VEGFR-1/2, activating downstream signaling to promote angiogenesis.

VEGFR

VEGFRs are VEGF receptors consisting of VEGFR-1, VEGFR-2 and VEGFR-3. VEGFR-1/2 are mainly expressed on tumor vascular endothelium and mediate tumor angiogenesis, while VEGFR-3 is primarily localized on lymphatic endothelium and regulates lymphangiogenesis.

Compared to the above clinical probes, developing effective fluorescent probes for colorectal cancer requires a chemical design strategy that meets three key needs: 1) real-time visualization via tumor-specific fluorescence activation, shown by probe **14**, which converts to a photosensitizer emitting at 635 nm; 2) high-sensitivity detection of sub-6 mm lesions through targeted molecular interactions, as seen with probe **15** (a c-Met-binding peptide-Cy5 conjugate) and probe **16** (an integrin-targeting cRGD-ZW800-1 system); and 3) surgical utility with near-infrared tissue penetration and anatomical guidance. These probes have improved pharmacokinetics, with lipophilic modifications in probe **14** allowing a 10–20-fold dose reduction and zwitterionic engineering in probe **16** to lower nonspecific uptake. Despite these advances, challenges persist in activating poorly differentiated cancers and



maintaining specificity for wound tissues, showing the need for next-generation designs that combine enzymatic activation with dual-targeting strategies.

View Article Online
DOI: 10.1039/D6SC02520J

2.4.3 Clinical probes for Digestive Glands

2.4.3.1 Liver

An early clinical study using probe **6** to identify liver tumors confirmed the feasibility of FGS for treating patients with hepatocellular carcinoma (HCC) and CRC metastasis, making it the earliest NIR probe approved by the Food and Drug Administration (FDA) for clinical application.⁸³ Intravenously injected, compound **6** accumulates in HCC and CRC metastatic lesions, emitting fluorescence to guide surgical resection, including occult small tumors. The design of **6**, combining targeted accumulation with fluorescence emission, drives its clinical success, demonstrated by 100% sensitivity and 93% positive predictive value for HCC and 100% sensitivity and 100% positive predictive value for CRC metastasis. The structural properties of **6** enable strong fluorescence and deep tissue penetration (≈ 8 mm), allowing detection of minute tumors. Meanwhile, its low adverse event rate ($\approx 0.003\%$) highlights the safety of this strategy. Multispectral imaging equipment allows tumor fluorescence to be captured in both NIR-I and NIR-II windows (Fig. 5D b). The strategic use of NIR-II imaging enhances surgical precision by enabling physicians to switch between NIR-I and NIR-II fluorescence for comparison. Compared to NIR-I imaging, NIR-II imaging offers superior sensitivity (100% vs 90.63%) and positive predictive value (91.43% vs 90.63%). Moreover, the tumor-normal liver tissue ratio (5.33 vs 1.45) and tumor detection rate (56.41% vs 46.15%) are both higher with NIR-II imaging. This breakthrough allows detection of tumors deeper than 8 mm, overcoming the limitation of NIR-I imaging, which struggles to visualize deep liver tumors.

2.5 Clinical probes for reproductive system and urinary system

The reproductive system and urinary system are closely related and interact with each other in terms of anatomical structure and physiological function.^{139, 140} We provide a summary of the clinical applications and research progress (Fig. 6A) of fluorescent probes in the reproductive and urinary systems.

2.5.1 Clinical probes for reproductive system

The reproductive system is responsible for secreting sex hormones and reproducing offspring. Its tumor-prone organs include the breast, ovary, and prostate.¹⁴¹ However, facing the surgical resection of these cancers, conventional white-light surgery usually provides no satisfactory surgical results and usually causes tumor recurrence.¹⁴² Therefore, to better resect these tumors, fluorescent probes have been applied to their surgery.

2.5.1.1 Clinical probes for breast

In addition to the above applications, this is the first time that the micro-dose NIR probe **6** can noninvasively image lymph nodes and lymph pathways.⁸⁶ Probe **6** utilizes a molecular design that binds to interstitial proteins, forming 5-10 nm biomacromolecules. Such albumin complexes accumulate in tumor-positive lymph nodes through multiple mechanisms, including the EPR effect, SPARC-mediated uptake by tumor cells within lymph nodes, phagocytosis by lymph node macrophages, and impaired lymphatic drainage, thereby exhibiting favorable fluorescence imaging performance.¹⁴³ This structure allows the probe to selectively enter lymphatic capillaries and accumulate in sentinel lymph nodes (SLNs) for 1-2 hours. The structural choice behind **6** enables real-time visualization of lymph drainage (Fig. 6C c) with high sensitivity (88.9%) and safety, offering a significant advantage over traditional blue dyes. However, the lack of specificity for lymph nodes and tumors reveals a limitation of this strategy, highlighting the need for more targeted designs—such as peptide-fluorophore conjugates—to enhance precision. While NIR fluorophores like **6** are useful for SLN tracing in breast cancer, the strategy of visualizing invisible fluorescence requires specialized imaging systems. To address this challenge, advanced imaging systems are needed to translate NIR signals into actionable surgical guidance within the anatomical context. The FLARE™



system was developed with this strategy in mind, combining the NIR signals with surgical anatomy.⁸⁷ Using ICG:HSA—a pre-complexed form of **6** with human serum albumin (Fig. 6C a)—FLARE™ provides real-time color video and NIR images, successfully identifying SLNs with 100% sensitivity (Fig. 6C b). This design significantly reduces surgical time, as ICG:HSA reaches SLNs in about 5 minutes, while allowing for real-time lymph flow

[View Article Online](#)

[DOI: 10.1039/D6SC02520J](https://doi.org/10.1039/D6SC02520J)



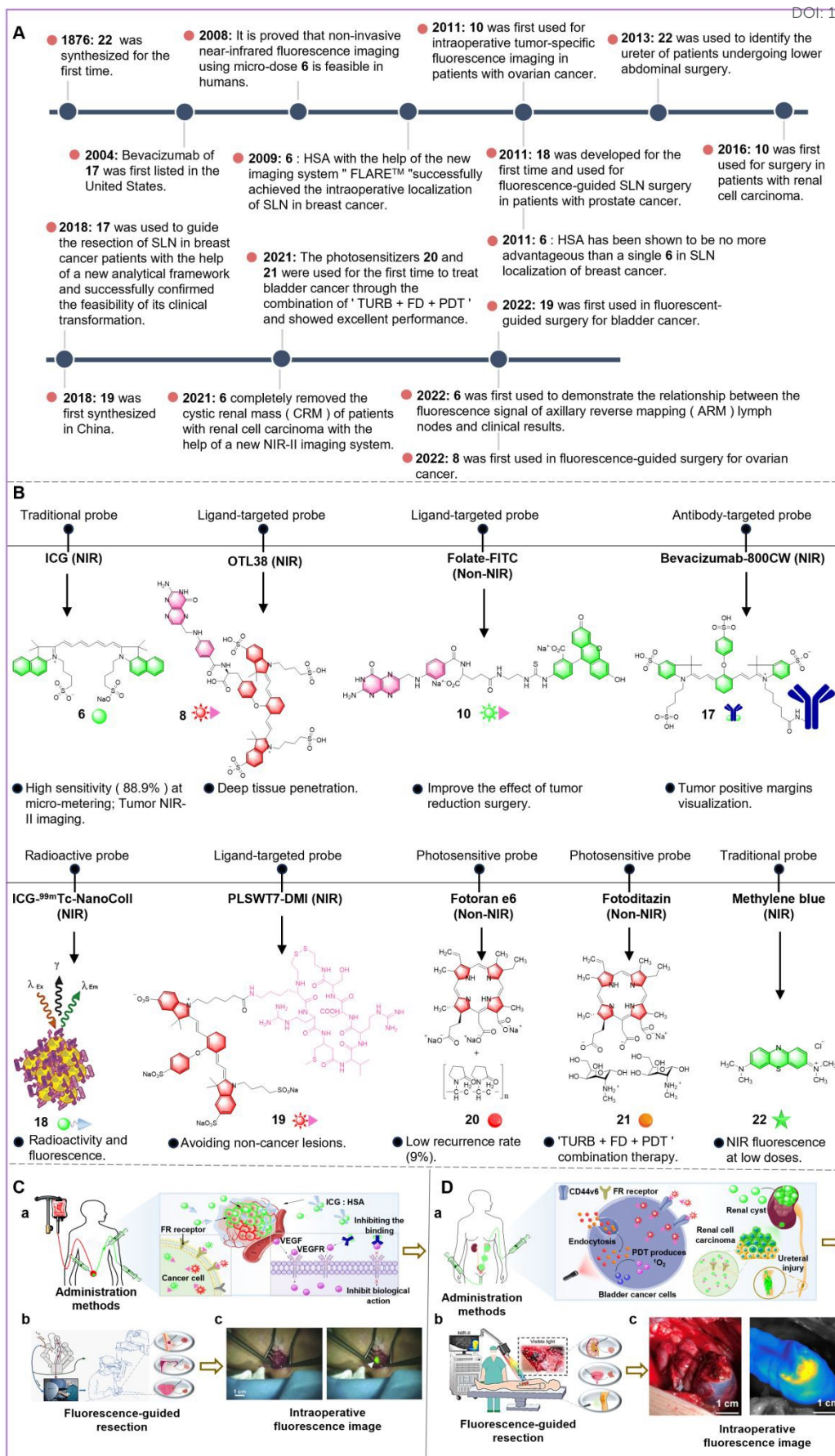


Fig. 6 (A) The timeline of research progress of fluorescent probes in the reproductive system and urinary system. (B) The chemical structures,



categories, and clinical efficacies of the probes. (C, D) Administration methods, *in vivo* fluorescence mechanisms, intraoperative fluorescence-guided resection methods, and clinical fluorescence images during surgery of the probes. (B 18 and C b) Reproduced from ref. 91 with permission from Elsevier Ltd, copyright 2011. (C c) Reproduced from ref. 144 with permission from Springer International Publishing, copyright 2012. (D b, c) Reproduced from ref. 93 with permission from John Wiley & Sons, Inc., copyright 2021.

without altering the surgical view. Given the limitations in device size and cost, the development of the more portable Mini-FLARE™ reflects an adaptation of this strategy to improve accessibility and convenience.

To further optimize clinical application, a comparative study utilizing the Mini-FLARE™ system was conducted to determine whether ICG:HSA offers superior performance over single probe **6**.⁸⁵ A randomized double-blind study compared ICG:HSA and **6** for SLN imaging in breast cancer. Using Mini-FLARE, results showed that single **6** provided higher fluorescence intensity and clearer lymph-vessel visibility than ICG:HSA, with no difference in SLN detection count. Consequently, single **6** is recommended for breast cancer to save costs. However, ICG:HSA remains superior in other cancers like hepatocellular carcinoma, likely because **6** sufficiently binds proteins during its longer transit to breast SLNs.¹⁴⁵

Compound **6** has been applied beyond sentinel lymph node mapping to axillary reverse mapping (ARM) for reducing complications in axillary lymph node dissection (ALND) in breast cancer.¹⁴⁶ The ARMONIC study demonstrated that ARM with probe **6** can effectively identify arm lymph nodes, with a high success rate of 94.5%, thereby reducing the risk of lymphedema. However, probe **6** exhibits low specificity. Metastatic and non-metastatic lymph nodes display comparable fluorescence signals, making it impossible to distinguish tumor-positive nodes from benign ones.⁸⁴ This highlights the need for more tumor-specific probes for better metastatic lymph node detection.

To address the lack of specificity with compound **6**, researchers have developed tumor-specific probes like **17** and established new analytical strategies for their clinical evaluation.⁸⁸ Targeting hypoxia-induced Vascular Endothelial Growth Factor-A (VEGF-A) overexpression in breast cancer, probe **17** is designed to provide specific NIR fluorescence for tumor imaging. The structure of **17** enables dose-independent specificity, successfully identifying tumor-positive margins in 88% of patients missed by traditional methods. Additionally, the IRDye800CW dye derived from probe **17** is predominantly excreted via the hepatobiliary system postoperatively, with no *in vivo* accumulation. This strategic design enhances pathological workflows by minimizing sampling errors and offering real-time guidance for precise resection. However, while the probe shows high clinical potential, the strategy of targeting VEGF-A still faces challenges, as false positives from parenchymal tissues like collagen need further investigation to improve specificity.

Based on previous reports, we believe the development of clinical breast cancer-targeted fluorescent probes should focus on three key issues: 1) Molecular target selectivity, low off-target rates, and multi-target compatibility. We propose using ligand-receptor conjugation technology. Targeting ligands like folate and Arg-Gly-Asp (RGD) peptides are covalently linked to near-infrared fluorophores such as Cy5.5 and IRDye800CW via amide bonds or click chemistry. This design ensures specific recognition of highly expressed receptors in breast cancer while reducing non-specific binding and adapting to the heterogeneity of different breast cancer types, especially triple-negative breast cancer. 2) Breast cancer probes must balance targeting specificity with optical performance. Probes should have a 650-900 nm near-infrared emission range for better tissue penetration and reduced autofluorescence. They should also have a quantum yield $\Phi > 0.3$, a large Stokes shift > 100 nm, and excellent photostability for sustained intraoperative laser use. These can be achieved through fluorophore molecular engineering, such as using squaraine dye SQ-660 for better quantum yield and designing electron donor-acceptor groups like D- π -A structured CY7-COOH to increase the Stokes shift. 3) Safe metabolic strategies and molecular design for biocompatible probes. To ensure safety, fluorescent probes must meet three biocompatibility requirements: rapid blood clearance (half-life



< 6 h), renal/hepatic dual-pathway excretion, and non-immunogenicity. We recommend a dual-track strategy: first, controlling the probe molecular weight for efficient clearance, such as with the GE11 peptide-ICG conjugate; second, optimizing surface modifications, such as PEGylation (e.g., PEG2000-Cy5.5) to reduce liver uptake and phosphorylcholine coating to avoid immune recognition. These designs will ensure clinical safety, as shown by the GE11-ICG system. 4) Chemical design and optimization for real-time intraoperative imaging. For precise navigation, probes must accumulate in tumors in < 30 minutes, provide persistent imaging for > 2 hours, show linear fluorescence intensity correlation with tumor burden, and be compatible with multi-modality imaging. The design of these fluorescent probes not only aids in the early detection of breast cancer but also optimizes the surgical process, enhances the precision of tumor removal, and reduces the risk of postoperative complications, providing safer and more effective surgical support for breast cancer patients.

2.5.1.2 Clinical probes for ovary

It is difficult to identify ovarian cancer by naked eyes and surgical experience of physicians during the surgery. In this regard, a tumor-specific fluorescent probe **10** was first applied to the cytoreductive surgery of ovarian cancer patients and achieved satisfactory visual effects.⁸⁹

Over 90% of ovarian cancers, particularly epithelial types, overexpress FR- α , making folate a key targeting ligand.¹⁴⁷ Probe **10**, designed by conjugating folate to Fluorescein 5-isothiocyanate (FITC: 525 nm) (Fig. 6B), is used intraoperatively: injected intravenously one hour before surgery, it binds FR- α and emits green fluorescence to guide cytoreductive surgery. The structure of **10** enables detection of all FR- α + tumors (100% identification rate), with stronger signals in well-differentiated tumors and the ability to detect deposits as small as 1 mm. However, its strategy of targeting FR- α limits specificity, as it fails on FR- α -negative tumors.

To improve on these limitations, novel near-infrared (NIR) probes with enhanced imaging capabilities have been developed for cytoreductive surgery. For example, **8** targets FR- α similarly to **10** but emits NIR light, which requires specialized equipment (Fig. 6C b).⁹⁰ The strategy behind **8** results in low autofluorescence, a higher tumor-to-background ratio (4.4 vs 3.1), and deeper tissue penetration (10 mm), allowing detection of deep and additional tumors (29% extra detection). Moreover, **8** has optimal kinetics with prolonged tumor retention (2-6 hours) and rapid plasma clearance (<2 hours). While **8** overcomes the previous limitations of **10**, its structure still leads to a 23% false positive rate due to FR- β expression in lymph node macrophages and FR- α in non-cancerous tissues, highlighting the need for further research.

The clinical management of ovarian cancer requires fluorescent molecular probes to meet several needs. We believe these can be addressed through innovative chemical strategies: 1) For early diagnosis and precise surgical navigation, probes must target specifically. This can be achieved by designing ligands such as PEGylated folate analogs targeting folate receptor α , and thiol-maleimide conjugated single-chain antibodies for mesothelin recognition. These modifications preserve natural ligand affinity while enabling controlled fluorescent labeling. 2) To address the deep pelvic location of the ovary, we recommend near-infrared fluorophores like cyanine derivatives, nitrogen-modified squaraine dyes, and D-A-D molecules with large Stokes shifts. These designs improve tissue penetration and reduce background interference. 3) For optimized pharmacokinetics, strategies should focus on controlling molecular weight, introducing hydrophilic groups (e.g., sulfonic acid or carboxyl groups for renal excretion), and designing responsive prodrugs (e.g., ROS/hypoxia-activated). 4) Multimodal compatibility can be achieved by integrating radiometal chelation sites or magnetic components. These innovations aim to improve ovarian cancer diagnosis and treatment by increasing sensitivity, specificity, and safety, ultimately enabling real-time tumor boundary visualization and complete resection assessment.



2.5.1.3 Clinical probes for prostate

View Article Online
DOI: 10.1039/D6SC02520J

During the surgery, it is important to detect and resect the SLN of prostate cancer.¹⁴⁸ Physicians can clear the surgical stage of the tumor and its metastatic pathway by the SLN of patients. Currently, **6** is the most widely used fluorescent probe for SLN detection in breast cancer patients.¹⁴⁹ However, due to the rapid *in vivo* migration of probe **6**, its distribution and metabolism cannot be accurately monitored, leading to incomplete SLN detection. This highlights the need for an accurate preoperative evaluation method in clinical practice. To address this, a hybrid multimodal radiocolloid, probe **18**, was developed for SLN detection in prostate cancer patients.⁹¹ This design strategy combines the fluorophore **6** with the radioactive drug ^{99m}Tc-NanoCol, giving **18** both radioactive and NIR fluorescence properties (Fig. 6B). The structure of **18** allows for detection by both lymphoscintigraphy and single-photon emission computed tomography/computed tomography (SPECT/CT) imaging before surgery, in addition to fluorescence imaging (Fig. 6C b). The NIR fluorescence from **6** enables real-time SLN imaging during surgery, allowing physicians to observe extra SLNs (about 22%) not seen with other preoperative methods. Additionally, fluorophore **6** is excreted via the hepatobiliary pathway. Moreover, the radioactivity from ^{99m}Tc-NanoCol aids in identifying SLN locations before surgery, assisting in accurate resection. Some SLNs (about 19%) are detected only by preoperative radioactivity detection, not by fluorescence imaging. **18** outperforms previous methods like ICG:HSA or **6** alone in SLN detection for prostate cancer, as shown in preclinical studies. However, prostate cancer fluorescence laparoscopy still requires manual adjustment, which can affect surgical accuracy. Thus, future studies should focus on improving probe tissue penetration and refining laparoscopic accuracy.

Table 4 Comparison of clinical and non-clinical probes in tumor targeting.

Type	Probe name	Mechanism type	Disease	Advantages / limitations	Refs.
Clinical probes					
Targeted probe	Panitumumab-IRDye800	Targeting EGFR	Glioma	High sensitivity and specificity; weak fluorescence in normal tissues; high biosafety.	54
	BLZ-100	Targeting CIC-3	Glioma	Deep tissue penetration; wide range of tumor recognition; clear tumor edge; high imaging stability.	64
Non-targeted probe	5-ALA	Active transport	Glioma	Clinical application is mature; high biosafety; low cost; easy to promote.	59
	ICG	Permeation	Glioma	Fast fluorescence effect; rapid metabolism in the body; deep tissue penetration.	150
Structural advantages from clinical probes					
<ul style="list-style-type: none"> ● The long linking bonds reduce the steric hindrance between the fluorescent probe and the targeted antibody. ● Water-soluble groups prevent hydrophobic aggregation of the probes. ● The symmetrical indole quaternary ammonium ring expands the conjugated range and constructs a rigid plane. 					
Non-clinical probes					
Targeted probe	NIR-Lys-H ₂ S	Identify H ₂ S	Glioma	It may target other H ₂ S-rich tissues, and its human BBB penetration remains unvalidated.	151
	MPA-Pip-abt-510	Targeting CD36	Glioma	Tumors (low-grade gliomas) with unobvious up-regulation of CD36 may be difficult to detect; the high molecular weight impedes intratumoral diffusion.	152
Non-targeted probe	IR780SS@CaP	Endocytosis	Peritoneal cancer	Risk of human accumulation; interference by tissue pH and GSH; unvalidated <i>in vivo</i> safety.	153
	BP-A	Diffusion	Breast cancer	Normal tissue aggregation risk; potential false-positive results.	154
Chemical challenges from non-clinical probes					
<ul style="list-style-type: none"> ● Large steric hindrance between the targeting part and the fluorescent group. ● Environmental sensitive groups have the possibility of non-specific activation <i>in vivo</i>. ● Non-specific recognition of endogenous substance recognition groups. 					

For deep-seated prostate cancer, the development of ultrasound or X-ray probes is crucial for treatment and surgical navigation due to tissue obstruction and limited optical imaging penetration. 1) Ultrasound probes can enhance acoustic reflection using microbubbles or nanobubbles. These probes consist of a gas core surrounded by a lipid or polymer shell, and their surfaces can be modified with targeting antigens like prostate-specific membrane



antigen (PSMA) for selective cancer cell targeting. Solid nanoparticles such as silicon, titanium, or calcium can improve acoustic contrast, while PEGylation or antibody conjugation boosts stability and targeting. 2) X-ray/CT probes use high atomic number elements to absorb X-rays. Small-molecule probes with iodine or tantalum can be linked to targeting ligands for cancer-specific accumulation. Gold, bismuth, or tantalum nanoparticles improve CT contrast and can also aid in photothermal or radiation-enhanced therapy. 3) Multimodal probes combining X-ray/CT with ultrasound or fluorescence provide preoperative localization, intraoperative navigation, and real-time monitoring. PSMA-targeted probes, tumor microenvironment-responsive probes, and nanoparticle carriers increase probe accumulation and signal in deep lesions while enabling drug delivery for integrated diagnosis and therapy. These strategies help locate deep prostate cancer and lymph nodes preoperatively, guide surgery in real-time, and offer therapeutic functions, improving clinical treatment accuracy and safety.

2.5.2 Clinical probes for urinary system

2.5.2.1 Clinical probes for Kidney

The main treatment of Renal Cell Carcinoma (RCC) is radical or partial nephrectomy, and its main presurgical diagnosis methods are MRI, CT and US.^{155, 156} However, these diagnostic methods cannot present the complete detection range, high-resolution imaging and real time imaging for RCC, thus leading to the incomplete resection of tumors and the residue of tumor-positive margins.¹⁵⁷ Clinically, probe **10** was first applied to tumor detection in patients with clear cell RCC, the most common subtype of RCC.⁹² Probe **10** targets FR- α , which is overexpressed in ovarian cancer and about 65% of clear cell RCC cases. This design competes with folate for FR- α binding (Fig. 6D a), achieving high tumor-to-background contrast (TBR~4.0) and ensuring no kidney parenchyma uptake, thus allowing precise resection of tumors and metastatic lymph nodes via real-time fluorescence imaging (Fig. 6D b). The non-ionizing property of probe **10** ensures safety, though its efficacy may be reduced if folate is ingested preoperatively. This strategy is particularly effective in nephron-sparing surgery, which preserves renal function by retaining nephrons.

With the advancement of NIR fluorescence, NIR-II imaging of probe **6** was developed for guiding cystic renal mass (CRM) resection.⁹³ After intravenous injection, **6** accumulates in tumors and SLNs, but not in the CRM liquid cavity. Instead, it highlights the surrounding renal parenchyma. The NIR-II system enables surgeons to clearly differentiate CRM from renal tissue, achieving near 100% complete resection in small patient studies (Fig. 6D c). The high fluorescence intensity (~6.37) and contrast-to-noise ratio (~5.25) greatly enhance visualization, reducing tumor-positive margins, which are often greater than 10% in traditional nephron-sparing surgery.

In order to allow more probes to be added to clinical trials, we compared the advantages of clinical probes and the limitations of non-clinical probes in tumor targeting (Table 4) and analyzed the structural advantages of clinical probes (Fig. 7). Clinical targeted probes, such as the EGFR-targeted Panitumumab-IRDye800 and CIC-3-targeted BLZ-100, possess high sensitivity, deep tissue penetration and favorable imaging stability. These superior performances benefit from rational structural optimization. Representative strategies include introducing long linkers to reduce steric hindrance, modifying hydrophilic groups to avoid aggregation, and constructing rigid conjugated planes to enhance fluorescence signals. Non-targeted clinical probes leverage established clinical utility and rapid metabolic clearance. In contrast, non-clinical probes like NIR-Lys-H₂S (H₂S-targeted) and MPA-Pip-abt-510 (CD36-targeted) face challenges including unverified BBB penetration and target heterogeneity, with chemical limitations such as poor tumor diffusion and nonspecific activation of environment-sensitive groups. Clearly, these identified challenges in non-clinical probes critically guide the optimization of next-generation clinical probes by highlighting key translational barriers in specificity, biodistribution, and safety.



2.5.2.2 Clinical probes for bladder

View Article Online
DOI: 10.1039/D6SC02520J

Bladder cancer is one of the most common malignant tumors of the human urinary system, its most common type is non-muscle invasive bladder cancer (NMIBC).¹⁵⁸ However, physicians usually ignore some small satellite tumors and flat tumors in situ under this method, which will cause the high recurrence rate (up to 70%) of NMIBC.¹⁵⁹ The NIR fluorescent probe **19** was developed and applied to the imaging of NMIBC patients for the first time and its clinical results are satisfactory.⁹⁴ Probe **19** exemplifies a rational molecular strategy that integrates target specificity and therapeutic potential through its structural design. The covalent conjugation of the high-affinity peptide PLSWT, which targets the N-terminal domain of CD44 variant 6 (CD44v6), with the near-infrared fluorophore IRDye800CW ensures stable *in vivo* binding via irreversible hyaluronic acid (HA) displacement, enabling real-time imaging with deep-tissue NIR emission (Fig. 6B). This structural strategy allows for selective accumulation in CD44v6-overexpressing tumors through competitive inhibition of endogenous HA binding, which disrupts the HA-CD44v6 interaction, both enabling tumor visualization and inhibiting oncogenic signaling and metastasis, offering a therapeutic advantage. The strategy behind probe **19** demonstrates significant clinical utility by providing high tumor-to-normal tissue contrast (TNR = 5.1) for real-time tumor delineation. It also detects satellite and flat lesions, reducing recurrence risk, and prevents unnecessary benign lesion resections, preserving bladder mucosa. Furthermore, unbound probe **19** is excreted via the hepatobiliary pathway with negligible *in vivo* accumulation. However, probe **19** cannot target tumors that do not express CD44v6, such as squamous cell carcinoma and adenocarcinoma, due to the varying expression of CD44v6 in different tumor types.¹⁶⁰



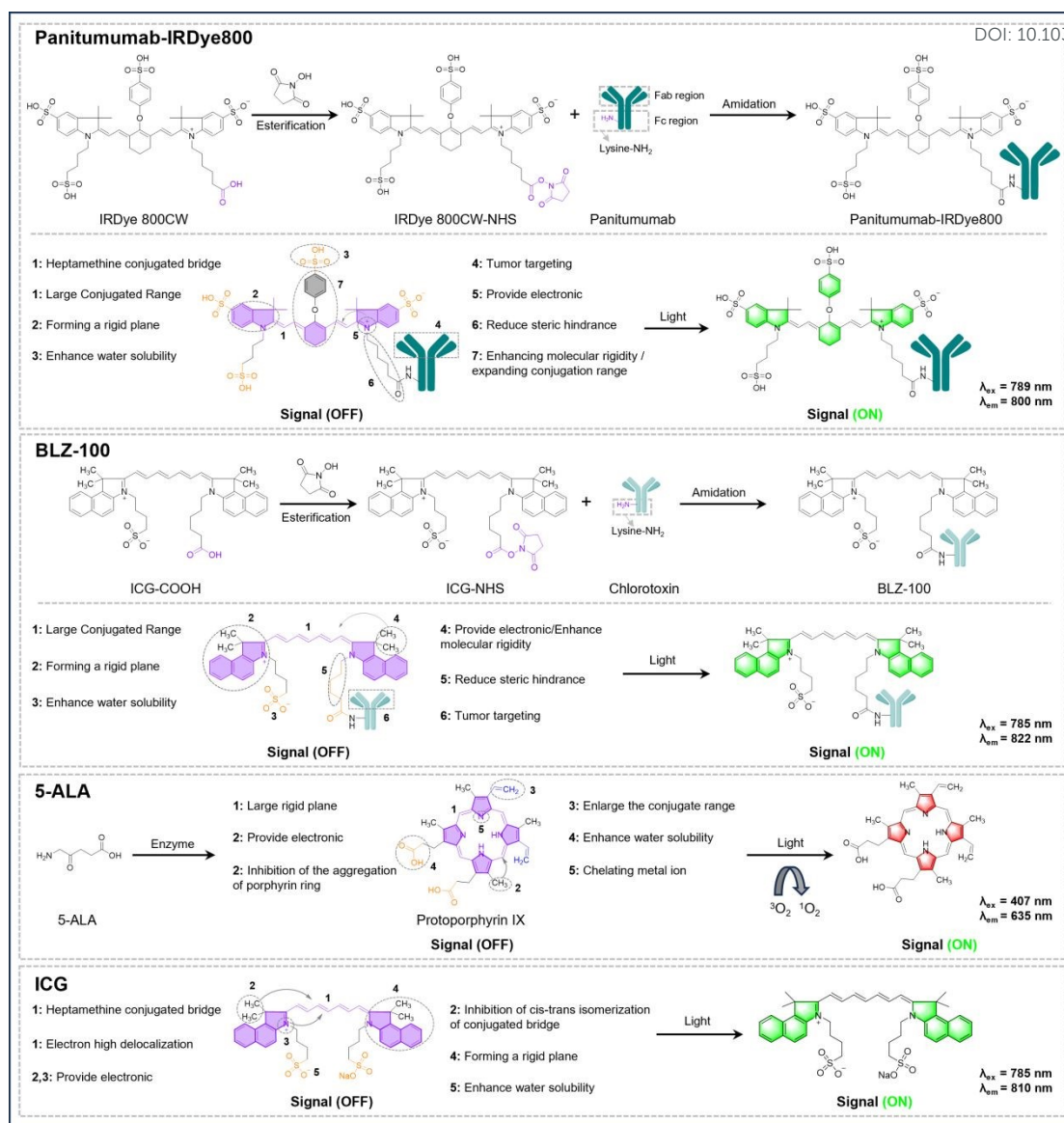


Fig. 7 Synthetic methods and structural analysis of panitumumab-IRDye800 (Probe 4; IRDye 800CW fluorophore), BLZ-100 (Probe 3; ICG fluorophore), 5-ALA (Probe 1; Protoporphyrin IX photosensitizer) and ICG (Probe 6; ICG fluorophore).

For the treatment of NMIBC in the clinic, transurethral resection of bladder tumor (TURBT) combined with intravesical chemotherapy (CT) or bacillus *Bacillus Calmette–Guérin* (BCG) is the surgical gold standard.^{161, 162} In recent years, a combined treatment of TURBT followed by fluorescence diagnosis (FD) and PDT was proposed and successfully used in the surgery of NMIBC.⁹⁵

This method integrates FD and PDT into traditional TURBT, incorporating new second-generation chlorin PSs **20** and **21** for PDT (Fig. 6B). The tetrapyrrolic ring structure of these photosensitizers (PSs) enables them to take advantage of the glutathione (GSH)-rich reductive tumor microenvironment typical of tumor cells. This redox potential difference drives selective endocytosis and accumulation within the cytosol of tumor cells, forming the chemical basis for subsequent diagnosis and therapy. In PDT, light irradiation at specific wavelengths triggers a Type II photochemical reaction, where excited-state PSs transfer energy to molecular oxygen ($^3\text{O}_2$), generating highly cytotoxic singlet oxygen ($^1\text{O}_2$). Compared to other second-generation PSs (e.g., Radachlorin, ALA, HLA), the chemical structure of **20** and **21** allows tumor-selective accumulation efficiency, a higher singlet oxygen quantum yield, and optimized photophysical properties, offering a prognostic advantage. These two photosensitizers are



mainly eliminated via the hepatobiliary pathway postoperatively, avoiding additional phototoxicity. Additionally, we compared the differences between clinical and non-clinical probes using different administration routes (Table 5), and analyzed the structural advantages of clinical probes (Fig. 8).

View Article Online

DOI: 10.1039/D6SC02520J

Table 5 Comparison of clinical and non-clinical probes in administration methods.

Type	Probes	Administration method	Disease	Advantages / limitations	Refs.
Clinical probes					
Systemic administration	OTL-38	Intravenous injection	lung cancer	Fast fluorescence signal; identifying deep lesions; high imaging contrast.	68
	cRGD-ZW800-1	Intravenous injection	Colon cancer	Low background fluorescence signal; high sensitivity of tumor; identify tumor and lymph node metastasis.	81
Topical administration	cMBP-ICG	Gargle	Oral cancer	Fast fluorescence effect; high tumor background ratio; simple way of administration.	76
	HAL	Enema	Rectal cancer	Low dose administration; no skin phototoxic reaction; patients with liver and kidney dysfunction are applicable.	79
Structural advantages from clinical probes					
<ul style="list-style-type: none"> • Ether bond connection improves stability. • The electron provided by the quaternary ammonium nitrogen atom increases the electron density of the conjugated system. • Molecular charge balance inhibits aggregation-induced quenching. 					
Non-clinical probes					
Systemic administration	Cy756-CHN-1	Intravenous injection	Breast cancer	Limited spatial resolution and deep penetration; potential background fluorescence interference.	163
	DCNP@PB	Intravenous injection	Colon cancer	Overreliance on the EPR effect; non-specific aggregation risk; unknown human circulatory stability.	164
Topical administration	YH-APN	Spray	Liver cancer	Off-target activation risk; tumor heterogeneity causes variable fluorescence performance.	165
	NIR-βgal-2	Spray	Breast cancer	Potential false positives; lack of standardized administration timing, dosage and imaging protocols.	166
Chemical challenges from non-clinical probes					
<ul style="list-style-type: none"> • The small delocalization range of electrons results in a large HOMO-LUMO energy gap. • Intramolecular rotation and vibration lead to high nonradiative transitions. • The lack of rigidity of the conjugated system leads to a decrease in fluorescence quantum yield. 					

To further enhance the efficacy of tumor-targeted therapies, it is essential to consider how the structural design of probes impacts both their performance and clinical applicability. The structural strategy differences between clinical and non-clinical probes directly determine their *in vivo* delivery properties and *in vivo* delivery efficiency. For clinical imaging probes, systematic structural optimization—such as incorporating ether linkages (-O-), introducing quaternary nitrogen centers, and achieving overall charge balance—can enhance molecular stability, suppress aggregation-induced quenching, and improve electronic density. These strategies lead to administration advantages, such as OTL-38, which benefits from structural stability for rapid fluorescence signal and deep lesion identification, and cRGD-ZW800-1 which reduces background fluorescence and enhances tumor sensitivity through charge balance design. Conversely, non-clinical probes are limited by structural defects, such as Cy756-CHN-1, which suffers from low spatial resolution due to insufficient electronic delocalization, and DCNP@PB, which faces non-specific aggregation and EPR dependence due to lack of rigidity. These structural limitations hinder their clinical applicability and administration efficacy.



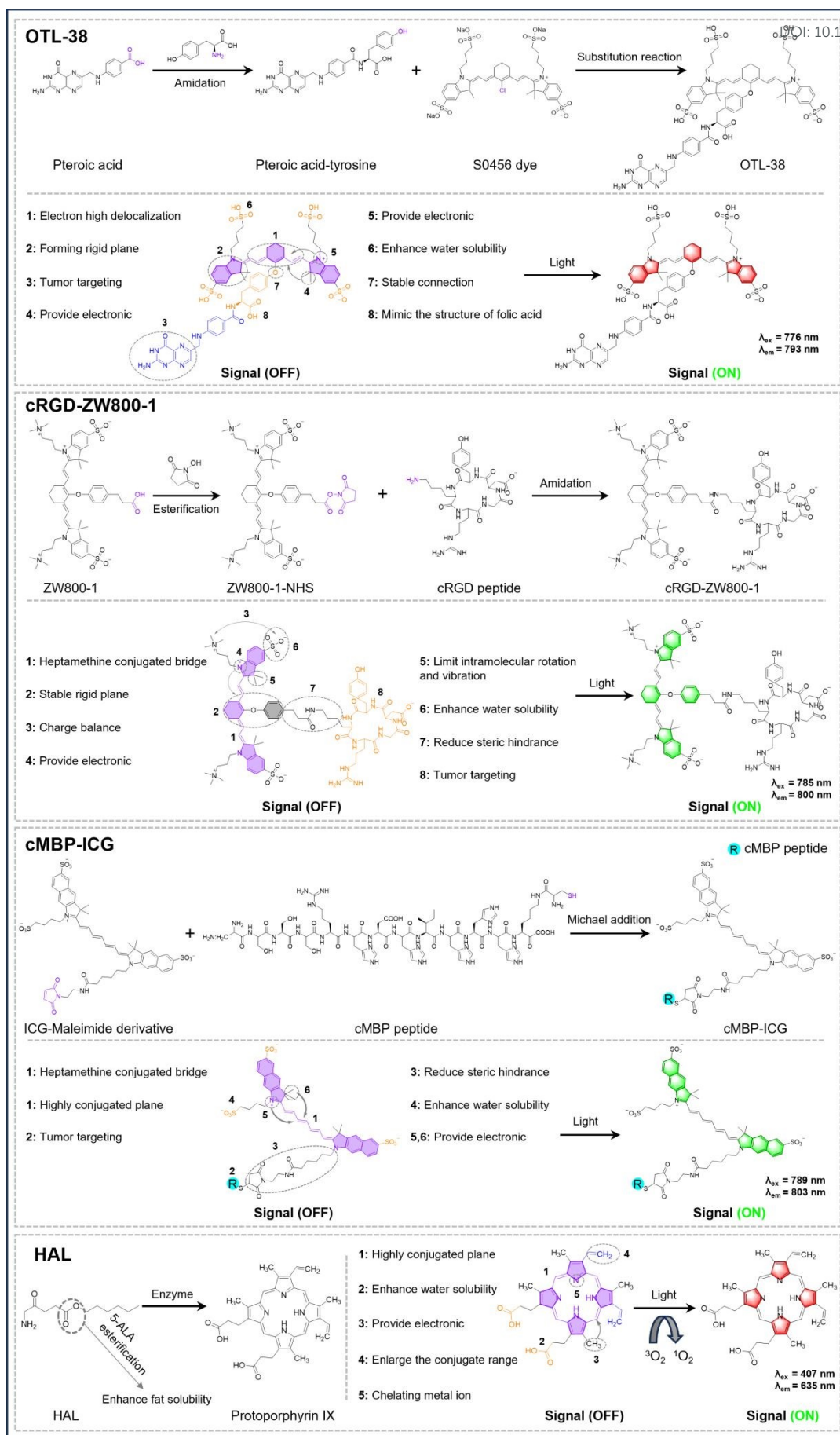


Fig. 8 Synthetic methods and structural analysis of OTL-38 (Probe 8; S0456 dye fluorophore), cRGD-ZW800-1 (Probe 16; ZW800-1 fluorophore),



cMBP-ICG (Probe 13; ICG fluorophore) and HAL (Probe 14; Protoporphyrin IX photosensitizer).

View Article Online
DOI: 10.1039/D6SC02520J

2.5.2.3 Clinical probes for ureter

The surgical sites of urinary system diseases are mainly in the lower abdomen of the human body. The surgeries of lower abdomen have a risk of iatrogenic injury for ureters, which may lead to some complications such as genitourinary fistula formation and serious kidney injury.¹⁶⁷ To avoid these complications, the low dose of probe **22** combined with NIR fluorescence imaging was first applied to the identification of the patient's ureters and showed satisfactory clinical results (Fig. 6D a, b).⁹⁶

The molecular design of fluorescent probe **22** follows three important strategies to optimize its intraoperative function, showing how structure determines properties and strategy determines advantages. 1) Its dilution-responsive NIR chromophore with a rigid molecular skeleton allows 700 nm fluorescence emission at low concentrations, maintaining high quantum yield. 2) Hydrophilic groups and controlled molecular weight enable glomerular filtration and ureter accumulation, providing real-time NIR imaging with high signal-to-noise ratio (4.59 ± 1.68). 3) Kinetically optimized structures ensure rapid onset within 10 minutes and prolonged retention for 60 minutes, providing sufficient imaging time. These features make probe **22** a safe, non-invasive alternative to radiation. However, limitations include renal clearance dependency, making it ineffective in kidney failure patients, and limited fluorescence penetration (3-5 mm), which hinders deep ureter imaging. Future improvements should focus on enhancing penetration and exploring hepatobiliary bypass.

Meanwhile, these limitations necessitate structural innovations to transcend existing constraints, a challenge addressed by advanced clinical probes in reproductive and urinary systems through tailored molecular architectures. Therefore, the structural advantages of clinical probes in the reproductive and urinary systems are worthy of reference and widespread adoption. We recommend that the following strategies are essential for improving the effectiveness and precision of clinical probes: 1) The heptamethine conjugated bridge forms a large conjugated plane, which endows the probes with significant near-infrared fluorescence in deep-seated tumors such as bladder and ovarian cancer. 2) Hydrophilic groups, such as sulfonate and carboxylate groups, prevent hydrophobic aggregation of the probes, resulting in stable fluorescence signals in tumor tissues. 3) For ICG, a probe that possesses both a hydrophobic structure and a negative charge from its sulfonic acid groups, it is able to bind to the hydrophobic pocket of albumin. This allows it to have a longer circulation time in the blood for angiography. 4) For methylene blue (MB), a small molecule with a small molecular weight and a rigid conjugated plane, like, phenothiazine structure, has an absolute advantage in ureteral imaging. The structural design will ensure the enhanced specificity, sensitivity, and clinical applicability, thereby paving the way for more effective and non-invasive cancer treatments.

3 Conclusion and Outlook

3.1 Mechanistic basis of clinical targeting across organ systems

Fluorescent probes are central to FGS, enabling real-time visualization, molecular selectivity, and intraoperative precision. Clinically, their mechanisms of action vary by organ system:

1) In the nervous system, probes typically exploit transporters (e.g., PEPT1/2), membrane channels, or EGFR to achieve tumor-selective uptake and enzyme-activated fluorescence.

2) In the circulatory system, probes bind endogenous albumin or lipoproteins, facilitating passive delivery into lipid-rich, macrophage-enriched, or hemorrhagic sites.

3) In the respiratory system, folate conjugation enables FR- α targeting, formulation engineering improves intratumoral retention, and cathepsin-activated designs provide enzyme-responsive “turn-on” signals.

4) In the digestive system, PARP1-, c-Met-, and integrin-targeted probes selectively illuminate malignant tissues by engaging DNA-repair pathways or surface receptor overexpression.



5) In the reproductive system, albumin-binding probes are trafficked to sentinel lymph nodes, while VEGF-A targeted designs modulate tumor angiogenesis.

6) In the urinary system, CD44v6-targeted probes achieve high-fidelity localization through selective receptor recognition.

3.2 Classification frameworks for clinical probes

Based on the fluorescence principle, unique characteristics, and administration methods of these fluorescent probes, we classify them as follows:

1) Targeting vs. non-targeting: Targeting probes use biomarker recognition (e.g., EGFR, FR- α , c-Met) for selective tumor accumulation, while non-targeting probes rely on physicochemical properties but lack specificity.

2) Systemic vs. topical administration: Systemic delivery is common, while topical administration is preferred for surface-accessible tumors (e.g., oral, gastric, breast, bladder) to reduce off-target diffusion and speed up probe accumulation.

3) NIR vs. non-NIR: NIR probes, especially NIR-II (1000-1700 nm), provide deeper tissue penetration, lower autofluorescence, and better contrast compared to visible or NIR-I probes.

4) Photosensitizer vs. non-photosensitizer: photosensitizing probes combine imaging and phototherapy by generating reactive oxygen species upon light exposure, enabling both tumor navigation and image-guided treatment.

3.3 System-specific clinical benefits of fluorescent probes

Clinically, the above mechanistic features offer distinct advantages for tumor visualization and resection across different organ systems:

1) Nervous system – Improved resection: Fluorescence in glioma surgery enhances tumor margin delineation, increasing total resection and reducing reoperation rates (e.g., FDA-approved probe 1).

2) Circulatory system – Imaging-guided PDT: Photosensitizer probes provide dual imaging and photodynamic therapy, benefiting vascular tumors like angiosarcoma (e.g., probe 5).

3) Respiratory system – Deep lesion detection: NIR probes penetrate deep tissue (≈ 10 mm) for detecting sub-centimeter lung nodules (e.g., probes 6, 8, 9).

4) Digestive system – Minimized surgical injury: Accurate margin identification reduces biopsies and preserves organ function in oral and colorectal cancers (e.g., probes 4 and 16).

5) Reproductive system – SLN mapping: Fluorescent probes identify sentinel lymph nodes in breast cancer, aiding staging and metastasis assessment (e.g., FDA-approved probe 6).

6) Urinary system – Enhanced visualization: Fluorescence improves tumor detection in bladder cancer and enables ureter identification to prevent injury (e.g., probes 19 and 22).

3.4 Clinical trade-offs of fluorescent probes

Clinically applicable fluorescent probes require excellent fluorescent and clinical performance, with the following key trade-offs:

1) Sensitivity vs. Specificity: High-sensitivity probes may have poor target specificity, causing nonspecific uptake and false positives. Clinically, prioritize sensitivity for early screening, small or deep lesions to avoid missed diagnosis, and specificity for diagnosis, intraoperative navigation and boundary delineation to prevent normal tissue injury.

2) Penetration Depth vs. Spatial Resolution: Long-wavelength probes have deep tissue penetration but lower quantum yield (vs. short-wavelength probes), leading to weak signals and poor SNR, due to smaller energy level differences facilitating non-radiative transitions. Future studies should optimize fluorophore structures (e.g., rigid conjugated planes) to enhance quantum yield and spatial resolution.



3) Stability vs. Responsiveness: Probes with high *in vivo* circulation stability (e.g., hydrophobic modification, core-shell structure) may reduce tumor microenvironment (pH, GSH, enzymes) response rate. Excessive responsiveness causes premature circulation triggering and reduced specificity. Probes with appropriate response thresholds should be designed to balance stability and responsiveness.

4) Metabolic Clearance vs. Imaging Time: Rapid clearance (hepatobiliary/renal pathways) reduces probe accumulation, phototoxicity and long-term side effects, but overly rapid metabolism shortens effective imaging time. Balance based on surgical duration: prioritize rapid clearance for short surgeries; optimize pharmacokinetics (PEGylation, hydrophilic-hydrophobic balance) to extend imaging time for complex deep tumor surgeries.

5) Signal Intensity vs. Biocompatibility: Enhancing *in vivo* signal often requires nanocarriers, radioactive groups or high fluorescent loading, but excessive modification increases biotoxicity, immunogenicity and accumulation risk. Signal intensity should be improved on the basis of high biocompatibility.

6) Synthesis/Usage Cost vs. Performance: High-performance probes involve complex synthesis and usage, increasing large-scale application costs. Clinical probes should simplify synthesis, reduce costs, and maintain high performance while ensuring process feasibility and batch stability.

3.5 Remaining obstacles and opportunities for translation

Though these advantages are accelerating the clinical translation of fluorescent probes, several key challenges remain:

1) Tumor targeting: Many current probes (e.g., ICG, 5-ALA, MB) lack strong molecular specificity. Future progress depends on finding new tumor receptors or engineering high-affinity ligands and antibodies (e.g., EGFR, FR- α , c-Met).

2) NIR-II imaging (1000-1700 nm): NIR-II probes show excellent penetration and contrast but are still in early stages. Expanding clinical trials with emerging NIR-II candidates (e.g., BTC980, BTC1070) is key.

3) Tumor-targeted photosensitizers: Current photosensitizers often lack selectivity and cause off-target effects. Third-generation, receptor-targeted photosensitizers and AIE-based platforms offer strong potential for precise imaging and phototherapy.

4) Other translational considerations: Safety, cost, and ease of use are crucial for real-world adoption, as probes must be both surgeon-friendly and acceptable to patients.

Acknowledgements

This work was supported by the National Natural Science Foundation of China (22174090); the Natural Science Basic Research Program of Shaanxi (2022JM-089); Long-term Project of high-level talents innovation in Shaanxi Province (Guang Chen); the High-end project of National Foreign Expert Program (H20250787; G2021041002L) and the Laoshan Laboratory (LSKJ202501700), and the Key R&D Plan of Hubei Province for local special support in the field of general health (No. 2022BCE066). J.Y. thanks to the Nano & Material Technology Development Program through the National Research Foundation of Korea (NRF) funded by Ministry of Science and ICT (RS-2024-00407093) and the National Research Foundation of Korea (NRF) grant funded by the Korea government (MSIT) (No. 2022R1A2C3005420). Open Deepseek (0528) tools was used as an auxiliary tool to polish the English contained in the first draft of this manuscript.

Author Contributions

Qiao Liang and Baolei Fan edited the original draft. Wenfang Jin and Yuxia Liu contributed to the scientific illustrations and clues in the manuscript. Dongliang Su provides the resources, funding support and clinical information toward market. Pu Chen and Juyoung Yoon created outline, conceptions and organization ideas for the review paper. Bo Tang and Guang Chen conceived the topic, organized the content and revised the manuscript. All

View Article Online

DOI: 10.1039/D6SC02520J



authors contributed to the final checking of the manuscript.

View Article Online
DOI: 10.1039/D6SC02520J

Conflict of interest

The authors declare no conflict of interest.

References

1. S. T. Barry, D. I. Gabrilovich, O. J. Sansom, A. D. Campbell and J. P. Morton, Therapeutic targeting of tumour myeloid cells, *Nat. Rev. Cancer*, 2023, **23**, 216-237.
2. X. Li, J. F. Lovell, J. Yoon and X. Chen, Clinical development and potential of photothermal and photodynamic therapies for cancer, *Nat. Rev. Clin. Oncol.*, 2020, **17**, 657-674.
3. A. Maeda, K. Uchita, T. Iwasaki and H. Yamai, Combination of endoscopic full-thickness resection and laparoscopic intragastric surgery for gastric submucosal tumor, *Endoscopy*, 2023, **55**, E1195-e1196.
4. P. R. Pandey, K. H. Young, D. Kumar and N. Jain, RNA-mediated immunotherapy regulating tumor immune microenvironment: next wave of cancer therapeutics, *Mol. Cancer*, 2022, **21**, 58.
5. Z. Zhu, Q. Xu, H. Yu, Q. Zhang, N. Jiang, L. Zhan, D. Zong, J. Wu, X. He, W. Peng, X. Li, L. Wang, M. Shi, X. Zhu and C. Chen, Effect of immunotherapy combined with chemotherapy with or without thoracic radiotherapy on markers of myocardial injury in patients with thoracic tumors, *J. Clin. Oncol.*, 2023, **41**, e14624-e14624.
6. O. Murphy, P. Forget, D. Ma and D. J. Buggy, Tumour excisional surgery, anaesthetic-analgesic techniques, and oncologic outcomes: a narrative review, *Br. J. Anaesth.*, 2023, **131**, 989-1001.
7. M. W. Lee, S. Han, K. Gu and H. Rhim, Local Ablation Therapy for Hepatocellular Carcinoma: Clinical Significance of Tumor Size, Location, and Biology, *Invest. Radiol.*, 2025, **60**, 53-59.
8. D. J. Erstad, M. Blum, J. S. Estrella, P. Das, B. D. Minsky, J. A. Ajani, P. F. Mansfield, N. Ikoma and B. D. Badgwell, Navigating Nodal Metrics for Node-Positive Gastric Cancer in the United States: An NCDB-Based Study and Validation of AJCC Guidelines, *J. Natl. Compr. Canc. Netw.*, 2021, **19**, 1-12.
9. R. V. Iyer, A. Hanlon, B. Fowble, G. Freedman, N. Nicolaou, P. Anderson, J. Hoffman, E. Sigurdson, M. Boraas and M. Torosian, Accuracy of the extent of axillary nodal positivity related to primary tumor size, number of involved nodes, and number of nodes examined, *Int. J. Radiat. Oncol. Biol. Phys.*, 2000, **47**, 1177-1183.
10. H. Pimentel, H. Jarnagin, H. Zong, C. Todorov, C. M. Anderson, B. Zhang, C. Bunker and X.-J. Ma, Preclinical CAR-T cell target safety, biodistribution, and tumor infiltration analysis using in situ hybridization technology, *J. Clin. Oncol.*, 2019, **37**, 112-112.
11. C. A. Iacobuzio-Donahue, K. Litchfield and C. Swanton, Intratumor heterogeneity reflects clinical disease course, *Nat. Cancer*, 2020, **1**, 3-6.
12. J. A. Wilcox, U. N. Chukwueke, M. J. Ahn, A. A. Aizer, T. A. Bale, D. Brandsma, P. K. Brastianos, S. Chang, M. Daras, P. Forsyth, L. Garzia, M. Glantz, I. C. G. Oliva, P. Kumthekar, E. Le Rhun, S. Nagpal, B. O'Brien, E. Pentsova, E. Q. Lee, J. Remsik, R. Rudà, I. Smalley, M. D. Taylor, M. Weller, J. Wefel, J. T. Yang, R. J. Young, P. Y. Wen and A. A. Boire, Leptomeningeal metastases from solid tumors: A Society for Neuro-Oncology and American Society of Clinical Oncology consensus review on clinical management and future directions, *Neuro Oncol.*, 2024, **26**, 1781-1804.
13. M. Taghiakbari, J. C. Anderson, D. von Renteln, S. Hirschmann, B. Jobse and H. Pohl, Extent of normal polyp resection margin: a possible quality measure for polyp resection, *Gut*, 2024, **73**, 216-218.



14. E. Picetti, F. S. Taccone and C. Robba, Craniectomy or Craniotomy for Acute Subdural Hematoma, *View Article Online Engl. J. Med.*, 2023, **389**, 862-863. DOI: 10.1039/D6SC02520J
15. K. A. Touijer, E. A. Vertosick, D. D. Sjoberg, N. Liso, S. Nalavenkata, B. Melao, V. P. Laudone, B. Ehdaie, B. Carver, J. A. Eastham, P. T. Scardino and A. J. Vickers, Pelvic Lymph Node Dissection in Prostate Cancer: Update from a Randomized Clinical Trial of Limited Versus Extended Dissection, *Eur. Urol.*, 2025, **87**, 253-260.
16. P. Xu, B. Chen, A. Xu, D. Yuan, Y. Zhang and C. Liu, Initial Experience with Intracorporeal Laparoscopic Radical Cystectomy and Detaenial Sigmoid Neobladder Reconstruction, *Eur. Urol.*, 2021, **79**, 545-551.
17. S. L. Hervey-Jumper, Y. Zhang, J. J. Phillips, R. A. Morshed, J. S. Young, L. McCoy, M. Lafontaine, T. Luks, S. Ammanuel, S. Kakaizada, A. Egladyous, A. Gogos, J. Villanueva-Meyer, A. Shai, G. Warriar, T. Rice, J. Crane, M. Wensch, J. K. Wiencke, M. Daras, N. A. Oberheim Bush, J. W. Taylor, N. Butowski, J. Clarke, S. Chang, E. Chang, M. Aghi, P. Theodosopoulos, M. McDermott, A. S. Jakola, V. K. Kavouridis, N. Nawabi, O. Solheim, T. Smith, M. S. Berger and A. M. Molinaro, Interactive Effects of Molecular, Therapeutic, and Patient Factors on Outcome of Diffuse Low-Grade Glioma, *J. Clin. Oncol.*, 2023, **41**, 2029-2042.
18. X. Meng, X. Pang, K. Zhang, C. Gong, J. Yang, H. Dong and X. Zhang, Recent Advances in Near-Infrared-II Fluorescence Imaging for Deep-Tissue Molecular Analysis and Cancer Diagnosis, *Small*, 2022, **18**, e2202035.
19. Y. H. Quan, C. H. Oh, D. Jung, J. Y. Lim, B. H. Choi, J. Rho, Y. Choi, K. N. Han, B. M. Kim, C. Kim, J. H. Park and H. K. Kim, Evaluation of Intraoperative Near-Infrared Fluorescence Visualization of the Lung Tumor Margin With Indocyanine Green Inhalation, *JAMA Surg.*, 2020, **155**, 732-740.
20. A. J. V. Mézquita, F. Biavati, V. Falk, H. Alkadhi, R. Hajhosseiny, P. Maurovich-Horvat, R. Manka, S. Kozerke, M. Stuber, T. Derlin, K. M. Channon, I. Išgum, A. Coenen, B. Foellmer, D. Dey, R. Volleberg, F. G. Meinel, M. R. Dweck, J. J. Piek, T. van de Hoef, U. Landmesser, G. Guagliumi, A. A. Giannopoulos, R. M. Botnar, R. Khamis, M. C. Williams, D. E. Newby and M. Dewey, Clinical quantitative coronary artery stenosis and coronary atherosclerosis imaging: a Consensus Statement from the Quantitative Cardiovascular Imaging Study Group, *Nat. Rev. Cardiol.*, 2023, **20**, 696-714.
21. S. Segobin, R. A. M. Haast, V. J. Kumar, A. Lella, A. Alkemade, M. Bach Cuadra, E. J. Barbeau, O. Felician, G. Pergola, A. L. Pitel, M. Saranathan, T. Tourdias and M. Hornberger, A roadmap towards standardized neuroimaging approaches for human thalamic nuclei, *Nat. Rev. Neurosci.*, 2024, **25**, 792-808.
22. P. D. Tudosiu, W. H. L. Pinaya, P. Ferreira Da Costa, J. Dafflon, A. Patel, P. Borges, V. Fernandez, M. S. Graham, R. J. Gray, P. Nachev, S. Ourselin and M. J. Cardoso, Realistic morphology-preserving generative modelling of the brain, *Nat. Mach. Intell.*, 2024, **6**, 811-819.
23. F. Yu, A. Moehring, O. Banerjee, T. Salz, N. Agarwal and P. Rajpurkar, Heterogeneity and predictors of the effects of AI assistance on radiologists, *Nat. Med.*, 2024, **30**, 837-849.
24. X. Tan, Q. Ni, T. Luo, K. T. Nam, H. B. Cheng, P. J. Dyson, X. J. Liang and J. Yoon, Photoswitchable imaging contrast agents as an emerging frontier in precision bioimaging, *Chem. Soc. Rev.*, 2026, **55**, 2959-2993.
25. W. R. Armstrong, A. U. Kishan, K. M. Booker, T. R. Grogan, D. Elashoff, E. C. Lam, K. J. Clark, M. L. Steinberg, W. P. Fendler, T. A. Hope, N. G. Nickols, J. Czernin and J. Calais, Impact of Prostate-specific Membrane Antigen Positron Emission Tomography/Computed Tomography on Prostate Cancer Salvage



Radiotherapy Management: Results from a Prospective Multicenter Randomized Phase 3 Trial (PSMA-SRT NCT03582774), *Eur. Urol.*, 2024, **86**, 52-60. View Article Online
DOI: 10.1039/D6SC02520J

26. S. Feger and M. Dewey, Coronary Computed Tomography Angiography, *Jama*, 2020, **324**, 1455-1456.
27. K. U. Koch, I. K. Mikkelsen, U. S. Espelund, H. Angleys, A. Tietze, G. V. Oettingen, N. Juul, L. Østergaard and M. Rasmussen, Cerebral Macro- and Microcirculation during Ephedrine versus Phenylephrine Treatment in Anesthetized Brain Tumor Patients: A Randomized Clinical Trial Using Magnetic Resonance Imaging, *Anesthesiology*, 2021, **135**, 788-803.
28. S. Saadatmand, H. A. Geuzinge, E. J. T. Rutgers, R. M. Mann, D. B. W. de Roy van Zuidewijn, H. M. Zonderland, R. Tollenaar, M. B. I. Lobbes, M. Ausems, M. van 't Riet, M. J. Hooning, I. Mares-Engelberts, E. J. T. Luiten, E. A. M. Heijnsdijk, C. Verhoef, N. Karssemeijer, J. C. Oosterwijk, I. M. Obdeijn, H. J. de Koning and M. M. A. Tilanus-Linthorst, MRI versus mammography for breast cancer screening in women with familial risk (FaMRIsC): a multicentre, randomised, controlled trial, *Lancet Oncol.*, 2019, **20**, 1136-1147.
29. Z. Xie, J. Wang, Y. Luo, B. Qiao, W. Jiang, L. Zhu, H. Ran, Z. Wang, W. Zhu, J. Ren and Z. Zhou, Tumor-penetrating nanoplatform with ultrasound "unlocking" for cascade synergistic therapy and visual feedback under hypoxia, *J. Nanobiotechnology*, 2023, **21**, 30.
30. L. Bastiani, F. Paolicchi, L. Faggioni, M. Martinelli, R. Gerasia, C. Martini, P. Cornacchione, M. Ceccarelli, D. Chiappino, D. Della Latta, J. Negri, D. Pertoldi, D. Negro, G. Nuzzi, V. Rizzo, P. Tamburrino, C. Pozzessere, G. Aringhieri and D. Caramella, Patient Perceptions and Knowledge of Ionizing Radiation From Medical Imaging, *JAMA Netw. Open*, 2021, **4**, e2128561.
31. V. Pichler, R. P. Martinho, L. Temming, T. Segers, F. R. Wurm and O. Koshkina, The Environmental Impact of Medical Imaging Agents and the Roadmap to Sustainable Medical Imaging, *Adv. Sci.*, 2025, **12**, e2404411.
32. L. Saba and E. d'Aloja, Predictive techniques in medical imaging: opportunities, limitations, and ethical-economic challenges, *NPJ Digit. Med.*, 2025, **8**, 392.
33. K. Fujita and Y. Urano, Activity-Based Fluorescence Diagnostics for Cancer, *Chem. Rev.*, 2024, **124**, 4021-4078.
34. A. Sharma, P. Verwilst, M. Li, D. Ma, N. Singh, J. Yoo, Y. Kim, Y. Yang, J. H. Zhu, H. Huang, X. L. Hu, X. P. He, L. Zeng, T. D. James, X. Peng, J. L. Sessler and J. S. Kim, Theranostic Fluorescent Probes, *Chem. Rev.*, 2024, **124**, 2699-2804.
35. B. Zhang, J. Lu, X. Lin, J. Wang, Q. Li, T. Jin, Q. Shi, Y. Lu, J. Zhang, J. Deng, Y. Zhang, Y. Guo, J. Gao, H. Chen, Y. Yan, J. Wu, J. Gao, J. Che, X. Dong, Z. Gu and N. Lin, Injectable and Sprayable Fluorescent Nanoprobe for Rapid Real-Time Detection of Human Colorectal Tumors, *Adv. Mater.*, 2024, **36**, e2405275.
36. E. S. Hwang, P. Beitsch, P. Blumencranz, D. Carr, A. Chagpar, L. Clark, N. Dekhne, D. Dodge, D. L. Dyess, L. Gold, S. Grobmyer, K. Hunt, S. Karp, B. A. Lesnikoski, I. Wapnir and B. L. Smith, Clinical Impact of Intraoperative Margin Assessment in Breast-Conserving Surgery With a Novel Pegulicianine Fluorescence-Guided System: A Nonrandomized Controlled Trial, *JAMA Surg.*, 2022, **157**, 573-580.
37. L. J. Lauwerends, P. van Driel, R. J. Baatenburg de Jong, J. A. U. Hardillo, S. Koljenovic, G. Puppels, L. Mezzanotte, C. Löwik, E. L. Rosenthal, A. L. Vahrmeijer and S. Keereweer, Real-time fluorescence imaging in intraoperative decision making for cancer surgery, *Lancet Oncol.*, 2021, **22**, e186-e195.
38. J. G. de Wit, J. Vonk, F. J. Voskuil, S. de Visscher, K. P. Schepman, W. T. R. Hooghiemstra, M. D.



- Linssen, S. G. Elias, G. B. Halmos, B. E. C. Plaat, J. J. Doff, E. L. Rosenthal, D. Robinson, B. van der Vegt, W. B. Nagengast, G. M. van Dam and M. J. H. Witjes, EGFR-targeted fluorescence molecular imaging for intraoperative margin assessment in oral cancer patients: a phase II trial, *Nat. Commun.*, 2023, **14**, 4952.
39. J. K. A. Rinne, H. Huhta, T. Pinta, A. Turunen, A. Mattila, K. Tahkola, O. Helminen, P. Ohtonen, T. Rautio and J. Kössi, Indocyanine Green Fluorescence Imaging in Prevention of Colorectal Anastomotic Leakage: A Randomized Clinical Trial, *JAMA Surg.*, 2025, **160**, 486-493.
40. R. Pal, M. E. Hom, N. S. van den Berg, T. M. Lwin, Y. J. Lee, A. Prilutskiy, W. Faquin, E. Yang, S. V. Saladi, M. A. Varvares, E. L. Rosenthal and A. T. N. Kumar, First Clinical Results of Fluorescence Lifetime-enhanced Tumor Imaging Using Receptor-targeted Fluorescent Probes, *Clin. Cancer Res.*, 2022, **28**, 2373-2384.
41. R. Solidoro, A. Centonze, M. Miciaccia, O. M. Baldelli, D. Armenise, S. Ferorelli, M. G. Perrone and A. Scilimati, Fluorescent imaging probes for in vivo ovarian cancer targeted detection and surgery, *Med. Res. Rev.*, 2024, **44**, 1800-1866.
42. Z. Wang, C. Zhao, Y. Li, J. Wang, D. Hou, L. Wang, Y. Wang, X. Wang, X. Liu, H. Wang and W. Xu, Photostable Cascade-Activatable Peptide Self-Assembly on a Cancer Cell Membrane for High-Performance Identification of Human Bladder Cancer, *Adv. Mater.*, 2023, **35**, e2210732.
43. G. Obaid, J. P. Celli, M. Broekgaarden, A. L. Bulin, P. Uusimaa, B. Pogue, T. Hasan and H. C. Huang, Engineering photodynamics for treatment, priming and imaging, *Nat. Rev. Bioeng.*, 2024, **2**, 752-769.
44. G. L. Pedersen, M. S. Erikson, K. Mogensen, S. Rosthøj and G. G. Hermann, Outpatient Photodynamic Diagnosis-guided Laser Destruction of Bladder Tumors Is as Good as Conventional Inpatient Photodynamic Diagnosis-guided Transurethral Tumor Resection in Patients with Recurrent Intermediate-risk Low-grade Ta Bladder Tumors. A Prospective Randomized Noninferiority Clinical Trial, *Eur. Urol.*, 2023, **83**, 125-130.
45. Y. Y. Zhao, L. Lu, H. Jeong, H. Kim, X. Li, H. Zhang and J. Yoon, Enhancing biosafety in photodynamic therapy: progress and perspectives, *Chem. Soc. Rev.*, 2025, **54**, 7749-7768.
46. A. Harun, N. Bendele, M. I. Khalil, I. Vasquez, J. Djuanda, R. Posey, M. H. Rashid, G. F. Christopher, U. Bickel, V. Gruev, J. Tropp, P. F. Egan and I. Srivastava, 3D Tumor-Mimicking Phantom Models for Assessing NIR I/II Nanoparticles in Fluorescence-Guided Surgical Interventions, *ACS nano.*, 2025, **19**, 19757-19776.
47. D. Y. Hou, X. P. Li, Y. Z. Wang, P. Zhang, J. C. Wu, H. H. You, M. Y. Lv, S. A. Zhou, X. Liu, G. Zhang, H. W. An, H. Wang and W. Xu, Translational contrast agents for use in fluorescence image-guided tumor surgery, *Biomaterials*, 2025, **325**, 123549.
48. L. Chen, J. Zhang, C. Chi, W. Che, G. Dong, J. Wang, Y. Du, R. Wang, Z. Zhu, J. Tian, N. Ji, X. Chen and D. Li, Lower-grade gliomas surgery guided by GRPR-targeting PET/NIR dual-modality image probe: a prospective and single-arm clinical trial, *Theranostics*, 2024, **14**, 819-829.
49. C. M. Kiernan, G. Thomas, A. Patel, R. Fan, F. Ye, P. A. Willmon and C. C. Solórzano, Does the Use of Probe-based Near-infrared Autofluorescence Parathyroid Detection Benefit Parathyroidectomy?: A Randomized Single-center Clinical Trial, *Ann. Surg.*, 2023, **278**, 549-558.
50. M. Weller, P. Y. Wen, S. M. Chang, L. Dirven, M. Lim, M. Monje and G. Reifenberger, Glioma, *Nat. Rev. Dis. Primers*, 2024, **10**, 33.
51. J. Gojo and M. Preusser, Improving long-term outcomes in pediatric low-grade glioma, *Nat. Cancer*, 2024,

View Article Online

DOI: 10.1039/D6SC02520J



- 5, 533-535.
52. M. J. van den Bent, M. Geurts, P. J. French, M. Smits, D. Capper, J. E. C. Bromberg and S. M. Chang, Primary brain tumours in adults, *Lancet*, 2023, **402**, 1564-1579.
53. M. Nasir-Moin, L. I. Wadiura, V. Sacalean, D. Juros, M. Movahed-Ezazi, E. K. Lock, A. Smith, M. Lee, H. Weiss, M. Mütther, D. Alber, S. Ratna, C. Fang, E. Suero-Molina, S. Hellwig, W. Stummer, K. Rössler, J. A. Hainfellner, G. Widhalm, B. Kiesel, D. Reichert, M. Mischkulnig, R. Jain, J. Straehle, N. Neidert, O. Schnell, J. Beck, J. Trautman, S. Pastore, D. Pacione, D. Placantonakis, E. K. Oermann, J. G. Golfinos, T. C. Hollon, M. Snuderl, C. W. Freudiger, D. H. Heiland and D. A. Orringer, Localization of protoporphyrin IX during glioma-resection surgery via paired stimulated Raman histology and fluorescence microscopy, *Nat. Biomed. Eng.*, 2024, **8**, 672-688.
54. Q. Zhou, N. S. van den Berg, E. L. Rosenthal, M. Iv, M. Zhang, J. C. M. Vega Leonel, S. Walters, N. Nishio, M. Granucci, R. Raymundo, G. Yi, H. Vogel, R. Cayrol, Y. J. Lee, G. Lu, M. Hom, W. Kang, M. Hayden Gephart, L. Recht, S. Nagpal, R. Thomas, C. Patel, G. A. Grant and G. Li, EGFR-targeted intraoperative fluorescence imaging detects high-grade glioma with panitumumab-IRDye800 in a phase 1 clinical trial, *Theranostics*, 2021, **11**, 7130-7143.
55. Y. Bliesener, R. M. Lebel, J. Acharya, R. Frayne and K. S. Nayak, Pseudo Test-Retest Evaluation of Millimeter-Resolution Whole-Brain Dynamic Contrast-enhanced MRI in Patients with High-Grade Glioma, *Radiology*, 2021, **300**, 410-420.
56. T. F. Cloughesy, K. Petrecca, T. Walbert, N. Butowski, M. Salacz, J. Perry, D. Damek, D. Bota, C. Bettgowda, J. J. Zhu, F. Iwamoto, D. Placantonakis, L. Kim, B. Elder, G. Kaptain, D. Cachia, Y. Moshel, S. Brem, D. Piccioni, J. Landolfi, C. C. Chen, H. Gruber, A. R. Rao, D. Hogan, W. Accomando, D. Ostertag, T. T. Montellano, T. Kheoh, F. Kabbnavar and M. A. Vogelbaum, Effect of Vocimagene Amiretrorepvec in Combination With Flucytosine vs Standard of Care on Survival Following Tumor Resection in Patients With Recurrent High-Grade Glioma: A Randomized Clinical Trial, *JAMA Oncol.*, 2020, **6**, 1939-1946.
57. R. Drexler, R. Khatri, T. Sauvigny, M. Mohme, C. L. Maire, A. Ryba, Y. Zghaibeh, L. Dührsen, A. Salviano-Silva, K. Lamszus, M. Westphal, J. Gempt, A. K. Wefers, J. E. Neumann, H. Bode, F. Hausmann, T. B. Huber, S. Bonn, K. Jütten, D. Delev, K. J. Weber, P. N. Harter, J. Onken, P. Vajkoczy, D. Capper, B. Wiestler, M. Weller, B. Snijder, A. Buck, T. Weiss, P. C. Göller, F. Sahn, J. A. Menstel, D. N. Zimmer, M. B. Keough, L. Ni, M. Monje, D. Silverbush, V. Hovestadt, M. L. Suvà, S. Krishna, S. L. Hervey-Jumper, U. Schüller, D. H. Heiland, S. Hänzelmann and F. L. Riecklefs, A prognostic neural epigenetic signature in high-grade glioma, *Nat. Med.*, 2024, **30**, 1622-1635.
58. L. S. Hu, F. D'Angelo, T. M. Weiskittel, F. P. Caruso, S. P. Fortin Ensign, M. R. Blomquist, M. J. Flick, L. Wang, C. P. Sereduk, K. Meng-Lin, G. De Leon, A. Nespodzany, J. C. Urcuyo, A. C. Gonzales, L. Curtin, E. M. Lewis, K. W. Singleton, T. Dondlinger, A. Anil, N. B. Semmineh, T. Noviello, R. A. Patel, P. Wang, J. Wang, J. M. Eschbacher, A. Hawkins-Daarud, P. R. Jackson, I. S. Grunfeld, C. Elrod, G. L. Mazza, S. C. McGee, L. Paulson, K. Clark-Swanson, Y. Lassiter-Morris, K. A. Smith, P. Nakaji, B. R. Bendok, R. S. Zimmerman, C. Krishna, D. P. Patra, N. P. Patel, M. Lyons, M. Neal, K. Donev, M. M. Mrugala, A. B. Porter, S. C. Beeman, T. R. Jensen, K. M. Schmainda, Y. Zhou, L. C. Baxter, C. L. Plaisier, J. Li, H. Li, A. Lasorella, C. C. Quarles, K. R. Swanson, M. Ceccarelli, A. Iavarone and N. L. Tran, Integrated molecular and multiparametric MRI mapping of high-grade glioma identifies regional biologic signatures, *Nat. Commun.*, 2023, **14**, 6066.



59. W. Stummer, U. Pichlmeier, T. Meinel, O. D. Wiestler, F. Zanella and H. J. Reulen, Fluorescence-guided surgery with 5-aminolevulinic acid for resection of malignant glioma: a randomised controlled multicentre phase III trial, *Lancet Oncol.*, 2006, **7**, 392-401.
60. P. Walker, A. Finch, V. Wykes, C. Watts and D. Tennant, Effects of the tumour microenvironment on protoporphyrin IX accumulation in glioblastoma, *Neuro Oncol.*, 2021, **23**, iv20-iv20.
61. C. Dupont, M. Vermandel, H. A. Leroy, M. Quidet, F. Lecomte, N. Delhem, S. Mordon and N. Reyns, INtraoperative photoDYnamic Therapy for GliOblastomas (INDYGO): Study Protocol for a Phase I Clinical Trial, *Neurosurgery*, 2019, **84**, E414-e419.
62. P. Poorva, J. Mast, B. Cao, M. V. Shah, K. E. Pollok and J. Shen, Killing the killers: Natural killer cell therapy targeting glioma stem cells in high-grade glioma, *Mol. Ther.*, 2025, **33**, 2462-2478.
63. R. Xie, Z. Wu, F. Zeng, H. Cai, D. Wang, L. Gu, H. Zhu, S. Lui, G. Guo, B. Song, J. Li, M. Wu and Q. Gong, Retro-enantio isomer of angiopep-2 assists nanoprobe across the blood-brain barrier for targeted magnetic resonance/fluorescence imaging of glioblastoma, *Signal Transduct. Target. Ther.*, 2021, **6**, 309.
64. C. G. Patil, D. G. Walker, D. M. Miller, P. Butte, B. Morrison, D. S. Kittle, S. J. Hansen, K. L. Nufer, K. A. Byrnes-Blake, M. Yamada, L. L. Lin, K. Pham, J. Perry, J. Parrish-Novak, L. Ishak, T. Prow, K. Black and A. N. Mamelak, Phase 1 Safety, Pharmacokinetics, and Fluorescence Imaging Study of Tozuleristide (BLZ-100) in Adults With Newly Diagnosed or Recurrent Gliomas, *Neurosurgery*, 2019, **85**, E641-e649.
65. W. W. Chin, P. W. Heng, P. S. Thong, R. Bhuvanewari, W. Hirt, S. Kuenzel, K. C. Soo and M. Olivo, Improved formulation of photosensitizer chlorin e6 polyvinylpyrrolidone for fluorescence diagnostic imaging and photodynamic therapy of human cancer, *Eur. J. Pharm. Biopharm.*, 2008, **69**, 1083-1093.
66. J. W. Verjans, E. A. Osborn, G. J. Ughi, M. A. Calfon Press, E. Hamidi, A. P. Antoniadis, M. I. Papafaklis, M. F. Conrad, P. Libby, P. H. Stone, R. P. Cambria, G. J. Tearney and F. A. Jaffer, Targeted Near-Infrared Fluorescence Imaging of Atherosclerosis: Clinical and Intracoronary Evaluation of Indocyanine Green, *JACC. Cardiovasc. Imaging*, 2016, **9**, 1087-1095.
67. E. L. Rosenthal, L. S. Moore, K. Tipirneni, E. de Boer, T. M. Stevens, Y. E. Hartman, W. R. Carroll, K. R. Zinn and J. M. Warram, Sensitivity and Specificity of Cetuximab-IRDye800CW to Identify Regional Metastatic Disease in Head and Neck Cancer, *Clin. Cancer Res.*, 2017, **23**, 4744-4752.
68. J. D. Predina, A. D. Newton, C. Connolly, A. Dunbar, M. Baldassari, C. Deshpande, E. Cantu, 3rd, J. Stadanlick, S. A. Kularatne, P. S. Low and S. Singhal, Identification of a Folate Receptor-Targeted Near-Infrared Molecular Contrast Agent to Localize Pulmonary Adenocarcinomas, *Mol. Ther.*, 2018, **26**, 390-403.
69. J. Rho, J. W. Lee, Y. H. Quan, B. H. Choi, B. K. Shin, K. N. Han, B. M. Kim, Y. H. Choi, H. S. Yong and H. K. Kim, Fluorescent and Iodized Emulsion for Preoperative Localization of Pulmonary Nodules, *Ann. Surg.*, 2021, **273**, 989-996.
70. G. T. Kennedy, D. E. Holt, F. S. Azari, E. Bernstein, B. Nadeem, A. Chang, N. T. Sullivan, A. Segil, C. Desphande, E. Bensen, J. T. Santini, J. C. Kucharczuk, E. J. Delikatny, M. Bogyo, A. J. M. Egan, C. W. Bradley, E. Eruslanov, J. D. Lickliter, G. Wright and S. Singhal, A Cathepsin-Targeted Quenched Activity-Based Probe Facilitates Enhanced Detection of Human Tumors during Resection, *Clin. Cancer Res.*, 2022, **28**, 3729-3741.
71. G. T. Kennedy, F. S. Azari, A. Chang, B. Nadeem, E. Bernstein, A. Segil, A. Din, I. Marfatia, C. Desphande, O. Okusanya, J. Keating, J. Predina, A. Newton, J. C. Kucharczuk and S. Singhal, Comparative Experience of Short-wavelength Versus Long-wavelength Fluorophores for Intraoperative

View Article Online
DOI: 10.1039/D6SC02520J



- Molecular Imaging of Lung Cancer, *Ann. Surg.*, 2022, **276**, 711-719.
72. P. S. Thong, M. Olivo, W. W. Chin, R. Bhuvanewari, K. Mancer and K. C. Soo, Clinical application of fluorescence endoscopic imaging using hypericin for the diagnosis of human oral cavity lesions, *Br. J. Cancer*, 2009, **101**, 1580-1584.
73. F. J. Voskuil, S. J. de Jongh, W. T. R. Hooghiemstra, M. D. Linssen, P. J. Steinkamp, S. de Visscher, K. P. Schepman, S. G. Elias, G. J. Meersma, P. K. C. Jonker, J. J. Doff, A. Jorritsma-Smit, W. B. Nagengast, B. van der Vegt, D. J. Robinson, G. M. van Dam and M. J. H. Witjes, Fluorescence-guided imaging for resection margin evaluation in head and neck cancer patients using cetuximab-800CW: A quantitative dose-escalation study, *Theranostics*, 2020, **10**, 3994-4005.
74. R. W. Gao, N. T. Teraphongphom, N. S. van den Berg, B. A. Martin, N. J. Oberhelman, V. Divi, M. J. Kaplan, S. S. Hong, G. Lu, R. Ertsey, W. Tummers, A. J. Gomez, F. C. Holsinger, C. S. Kong, A. D. Colevas, J. M. Warram and E. L. Rosenthal, Determination of Tumor Margins with Surgical Specimen Mapping Using Near-Infrared Fluorescence, *Cancer Res.*, 2018, **78**, 5144-5154.
75. P. Demétrio de Souza França, S. Kossatz, C. Brand, D. Karassawa Zanoni, S. Roberts, N. Guru, D. Adilbay, A. Mauguen, C. Valero Mayor, W. A. Weber, H. Schöder, R. A. Ghossein, I. Ganly, S. G. Patel and T. Reiner, A phase I study of a PARP1-targeted topical fluorophore for the detection of oral cancer, *Eur. J. Nucl. Med. Mol. Imaging*, 2021, **48**, 3618-3630.
76. J. Wang, S. Li, K. Wang, L. Zhu, L. Yang, Y. Zhu, Z. Zhang, L. Hu, Y. Yuan, Q. Fan, J. Ren, G. Yang, W. Ding, X. Zhou, J. Cui, C. Zhang, Y. Yuan, R. Huang, J. Tian and X. Tao, A c-MET-Targeted Topical Fluorescent Probe cMBP-ICG Improves Oral Squamous Cell Carcinoma Detection in Humans, *Ann. Surg. Oncol.*, 2023, **30**, 641-651.
77. P. M. Lombardi, M. Mazzola, V. Nicastro, S. Giacomuzzi, G. L. Baiocchi, C. Castoro, R. Rosati, U. Fumagalli Romario, L. Bonavina, F. Staderini, I. Gockel, D. Gregori, P. De Martini, M. Gualtierotti, M. Danieli, S. Beretta, M. Mutignani, E. Forti and G. Ferrari, The iGreenGO Study: The Clinical Role of Indocyanine Green Imaging Fluorescence in Modifying the Surgeon's Conduct During the Surgical Treatment of Advanced Gastric Cancer-Study Protocol for an International Multicenter Prospective Study, *Front. Oncol.*, 2022, **12**, 854754.
78. M. Wei, Y. Liang, L. Wang, Z. Li, Y. Chen, Z. Yan, D. Sun, Y. Huang, X. Zhong, P. Liu and W. Yu, Clinical Application of Indocyanine Green Fluorescence Technology in Laparoscopic Radical Gastrectomy, *Front. Oncol.*, 2022, **12**, 847341.
79. E. Endlicher, C. M. Gelbmann, R. Knüchel, A. Fürst, R. M. Szeimies, S. K. Gölder, J. Schölmerich, C. Lottner and H. Messmann, Hexaminolevulinate-induced fluorescence endoscopy in patients with rectal adenoma and cancer: a pilot study, *Gastrointest. Endosc.*, 2004, **60**, 449-454.
80. J. Burggraaf, I. M. Kamerling, P. B. Gordon, L. Schrier, M. L. de Kam, A. J. Kales, R. Bendiksen, B. Indrevoll, R. M. Bjerke, S. A. Moestue, S. Yazdanfar, A. M. Langers, M. Swaerd-Nordmo, G. Torheim, M. V. Warren, H. Morreau, P. W. Voorneveld, T. Buckle, F. W. van Leeuwen, L. I. Ødegårdstuen, G. T. Dalsgaard, A. Healey and J. C. Hardwick, Detection of colorectal polyps in humans using an intravenously administered fluorescent peptide targeted against c-Met, *Nat. Med.*, 2015, **21**, 955-961.
81. K. S. de Valk, M. M. Deken, H. J. M. Handgraaf, S. S. Bhairosingh, O. D. Bijlstra, M. J. van Esdonk, A. G. T. Terwisscha van Scheltinga, A. Valentijn, T. L. March, J. Vuijk, K. Peeters, F. A. Holman, D. E. Hilling, J. S. D. Mieog, J. V. Frangioni, J. Burggraaf and A. L. Vahrmeijer, First-in-Human Assessment of cRGD-ZW800-1, a Zwitterionic, Integrin-Targeted, Near-Infrared Fluorescent Peptide in Colon

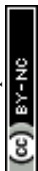


- Carcinoma, *Clin. Cancer Res.*, 2020, **26**, 3990-3998.
82. Z. Hu, C. Fang, B. Li, Z. Zhang, C. Cao, M. Cai, S. Su, X. Sun, X. Shi, C. Li, T. Zhou, Y. Zhang, C. Chi, P. He, X. Xia, Y. Chen, S. S. Gambhir, Z. Cheng and J. Tian, First-in-human liver-tumour surgery guided by multispectral fluorescence imaging in the visible and near-infrared-I/II windows, *Nat. Biomed. Eng.*, 2020, **4**, 259-271.
83. T. Ishizawa, N. Fukushima, J. Shibahara, K. Masuda, S. Tamura, T. Aoki, K. Hasegawa, Y. Beck, M. Fukayama and N. Kokudo, Real-time identification of liver cancers by using indocyanine green fluorescent imaging, *Cancer*, 2009, **115**, 2491-2504.
84. M. Abbaci, A. Conversano, M. Karimi, M. C. Mathieu, V. Rouffiac, F. De Leeuw, S. Michiels, C. Laplace-Builhé and C. Mazouni, Near-Infrared Fluorescence Axillary Reverse Mapping (ARM) Procedure in Invasive Breast Cancer: Relationship between Fluorescence Signal in ARM Lymph Nodes and Clinical Outcomes, *Cancers (Basel)*, 2022, **14**, 2614.
85. M. Hutteman, J. S. Mieog, J. R. van der Vorst, G. J. Liefers, H. Putter, C. W. Löwik, J. V. Frangioni, C. J. van de Velde and A. L. Vahrmeijer, Randomized, double-blind comparison of indocyanine green with or without albumin premixing for near-infrared fluorescence imaging of sentinel lymph nodes in breast cancer patients, *Breast Cancer Res. Treat.*, 2011, **127**, 163-170.
86. E. M. Sevick-Muraca, R. Sharma, J. C. Rasmussen, M. V. Marshall, J. A. Wendt, H. Q. Pham, E. Bonefas, J. P. Houston, L. Sampath, K. E. Adams, D. K. Blanchard, R. E. Fisher, S. B. Chiang, R. Elledge and M. E. Mawad, Imaging of lymph flow in breast cancer patients after microdose administration of a near-infrared fluorophore: feasibility study, *Radiology*, 2008, **246**, 734-741.
87. S. L. Troyan, V. Kianzad, S. L. Gibbs-Strauss, S. Gioux, A. Matsui, R. Oketokoun, L. Ngo, A. Khamene, F. Azar and J. V. Frangioni, The FLARE intraoperative near-infrared fluorescence imaging system: a first-in-human clinical trial in breast cancer sentinel lymph node mapping, *Ann. Surg. Oncol.*, 2009, **16**, 2943-2952.
88. M. Koller, S. Q. Qiu, M. D. Linssen, L. Jansen, W. Kelder, J. de Vries, I. Kruihof, G. J. Zhang, D. J. Robinson, W. B. Nagengast, A. Jorritsma-Smit, B. van der Vegt and G. M. van Dam, Implementation and benchmarking of a novel analytical framework to clinically evaluate tumor-specific fluorescent tracers, *Nat. Commun.*, 2018, **9**, 3739.
89. G. M. van Dam, G. Themelis, L. M. Crane, N. J. Harlaar, R. G. Pleijhuis, W. Kelder, A. Sarantopoulos, J. S. de Jong, H. J. Arts, A. G. van der Zee, J. Bart, P. S. Low and V. Ntziachristos, Intraoperative tumor-specific fluorescence imaging in ovarian cancer by folate receptor- α targeting: first in-human results, *Nat. Med.*, 2011, **17**, 1315-1319.
90. C. E. Hoogstins, Q. R. Tummers, K. N. Gaarenstroom, C. D. de Kroon, J. B. Trimbos, T. Bosse, V. T. Smit, J. Vuyk, C. J. van de Velde, A. F. Cohen, P. S. Low, J. Burggraaf and A. L. Vahrmeijer, A Novel Tumor-Specific Agent for Intraoperative Near-Infrared Fluorescence Imaging: A Translational Study in Healthy Volunteers and Patients with Ovarian Cancer, *Clin. Cancer Res.*, 2016, **22**, 2929-2938.
91. H. G. van der Poel, T. Buckle, O. R. Brouwer, R. A. Valdés Olmos and F. W. van Leeuwen, Intraoperative laparoscopic fluorescence guidance to the sentinel lymph node in prostate cancer patients: clinical proof of concept of an integrated functional imaging approach using a multimodal tracer, *Eur. Urol.*, 2011, **60**, 826-833.
92. T. J. Guzzo, J. Jiang, J. Keating, E. DeJesus, R. Judy, S. Nie, P. Low, P. Lal and S. Singhal, Intraoperative Molecular Diagnostic Imaging Can Identify Renal Cell Carcinoma, *J. Urol.*, 2016, **195**, 748-755.

View Article Online
DOI: 10.1039/D6SC02520J



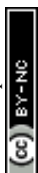
93. C. Cao, S. Deng, B. Wang, X. Shi, L. Ge, M. Qiu, F. Zhang, M. Lu, L. Ma, C. Chi, Z. Hu, J. Tian and S. Zhang, Intraoperative near-infrared II window fluorescence imaging-assisted nephron-sparing surgery for complete resection of cystic renal masses, *Clin. Transl. Med.*, 2021, **11**, e604. View Article Online
DOI: 10.1039/D6SC02520J
94. W. Shang, L. Peng, K. He, P. Guo, H. Deng, Y. Liu, Z. Chen, J. Tian and W. Xu, A clinical study of a CD44v6-targeted fluorescent agent for the detection of non-muscle invasive bladder cancer, *Eur. J. Nucl. Med. Mol. Imaging*, 2022, **49**, 3033-3045.
95. A. V. Kustov, N. L. Smirnova, O. A. Privalov, T. M. Moryganova, A. I. Strel'nikov, P. K. Morshnev, O. I. Koifman, A. V. Lyubim'tsev, T. V. Kustova and D. B. Berezin, Transurethral Resection of Non-Muscle Invasive Bladder Tumors Combined with Fluorescence Diagnosis and Photodynamic Therapy with Chlorin e(6)-Type Photosensitizers, *J. Clin. Med.*, 2021, **11**, 233.
96. F. P. Verbeek, J. R. van der Vorst, B. E. Schaafsma, R. J. Swijnenburg, K. N. Gaarenstroom, H. W. Elzevier, C. J. van de Velde, J. V. Frangioni and A. L. Vahrmeijer, Intraoperative near infrared fluorescence guided identification of the ureters using low dose methylene blue: a first in human experience, *J. Urol.*, 2013, **190**, 574-579.
97. N. Cabioglu, H. B. Koçer, H. Karanlık, M. A. Gülçelik, A. Igci, M. Müslümanoğlu, C. Uras, B. Mantoglu, D. C. Trabulus, G. Akgül, M. Tükenmez, K. Senol, E. Özkurt, E. Sen, G. Karadeniz Çakmak, S. Bademler, S. Emiroglu, N. Yildirim, H. Kara, A. Dag, E. Dilege, A. Altinok, G. Basaran, E. Varol, Ü. Ugurlu, Y. Bölükbaşı, Y. E. Ersoy, B. Zengel, N. Karaman, S. Özbas, L. Zer, H. Gül Kiliç, O. Agcaoglu, G. Sakman, Z. Utkan, A. Soyder, A. Akcan, S. Ergün, R. Yilmaz, A. Aydinler, A. Soran, K. Ibis and V. Özmen, De-Escalation of Nodal Surgery in Clinically Node-Positive Breast Cancer, *JAMA Surg.*, 2025, **160**, 257-266.
98. B. Ibanez, A. Fernández-Ortiz, L. Fernández-Friera, I. García-Lunar, V. Andrés and V. Fuster, Progression of Early Subclinical Atherosclerosis (PESA) Study: JACC Focus Seminar 7/8, *J. Am. Coll. Cardiol.*, 2021, **78**, 156-179.
99. C. A. Painter, E. Jain, B. N. Tomson, M. Dunphy, R. E. Stoddard, B. S. Thomas, A. L. Damon, S. Shah, D. Kim, J. Gómez Tejada Zañudo, J. L. Hornick, Y. L. Chen, P. Merriam, C. P. Raut, G. D. Demetri, B. A. Van Tine, E. S. Lander, T. R. Golub and N. Wagle, The Angiosarcoma Project: enabling genomic and clinical discoveries in a rare cancer through patient-partnered research, *Nat. Med.*, 2020, **26**, 181-187.
100. A. Hak, M. S. Ali, S. A. Sankaranarayanan, V. R. Shinde and A. K. Rengan, Chlorin e6: A Promising Photosensitizer in Photo-Based Cancer Nanomedicine, *ACS Appl. Bio Mater.*, 2023, **6**, 349-364.
101. T. Takahashi, Y. Miyazaki, T. Makino, Y. Kurokawa, M. Yamasaki, S. Takiguchi, K. Nakajima, M. Mori and Y. Doki, The clinical trial for photodynamic diagnosis mediated 5-ALA for peritoneal metastasis due to advanced gastric cancer, *J. Clin. Oncol.*, 2016, **34**, 71-71.
102. A. Cesaro, V. Acerbo, C. Indolfi, P. P. Filardi and P. Calabrò, The clinical relevance of the reversal of coronary atherosclerotic plaque, *Eur. J. Intern. Med.*, 2024, **129**, 16-24.
103. A. Fuchs, J. T. Kühn, P. E. Sigvardsen, S. Afzal, A. D. Knudsen, M. B. Møller, M. C. de Knegt, M. H. Sørgaard, B. G. Nordestgaard, L. V. Køber and K. F. Kofoed, Subclinical Coronary Atherosclerosis and Risk for Myocardial Infarction in a Danish Cohort: A Prospective Observational Cohort Study, *Ann. Intern. Med.*, 2023, **176**, 433-442.
104. H. W. West, K. Dangas and C. Antoniades, Advances in Clinical Imaging of Vascular Inflammation: A State-of-the-Art Review, *JACC. Basic Transl. Sci.*, 2024, **9**, 710-732.
105. N. M. Htun, Y. C. Chen, B. Lim, T. Schiller, G. J. Maghzal, A. L. Huang, K. D. Elgass, J. Rivera, H. G. Schneider, B. R. Wood, R. Stocker and K. Peter, Near-infrared autofluorescence induced by intraplaque



- hemorrhage and heme degradation as marker for high-risk atherosclerotic plaques, *Nat. Commun.*, 2017, **8**, 75. [View Article Online](#)
DOI: 10.1039/D6SC02520J
106. R. Guo, M. Deng, J. Li, X. He, P. He, H. Liu, Y. Ye, Z. Mo, X. He, M. Li and Q. He, Depriving Tumor Cells of Ways to Metastasize: Ferroptosis Nanotherapy Blocks Both Hematogenous Metastasis and Lymphatic Metastasis, *Nano Lett.*, 2023, **23**, 3401-3411.
107. D. Xie, J. Shen, L. Liu, B. Cao, A. Xiao, J. Qin, J. Wu, Q. Yan, Y. Hu, C. Yang, Z. Cao, J. Hu, P. Yin and J. Gong, Randomized clinical trial on D2 lymphadenectomy versus D2 lymphadenectomy plus complete mesogastric excision in patients undergoing gastrectomy for cancer (DCGC01 study), *Br. J. Surg.*, 2024, **111**, znze106.
108. R. Ratsihorimanana, T. Maitre, M. Dusselier, M. Triet Ngo, G. Mangiapan, C. Fournier, A. Bourdin, S. Jouneau, M. Matar, N. Favrolt, T. Egenod, J. M. Vergnon, D. Wermert, J. F. Boitiaux, R. Borie, R. Caliandro, O. Freynet, V. Gounant, J. Mankikian, J. Camuset, A. Elabbadi, A. Parrot, J. Calvani, M. Fortin, N. Guibert, V. Cottin and J. Cadranet, Recurrent respiratory papillomatosis in adults with lower respiratory tract involvement: a retrospective study of the OrphaLung and GETIF networks, *Eur. Respir. J.*, 2025, **65**, 2400618.
109. T. Cascone, M. M. Awad, J. D. Spicer, J. He, S. Lu, B. Sepesi, F. Tanaka, J. M. Taube, R. Cornelissen, L. Havel, N. Karaseva, J. Kuzdzal, L. B. Petruzella, L. Wu, J. L. Pujol, H. Ito, T. E. Ciuleanu, L. de Oliveira Muniz Koch, A. Janssens, A. Alexandru, S. Bohnet, F. V. Moiseyenko, Y. Gao, Y. Watanabe, C. Coronado Erdmann, P. Sathyanarayana, S. Meadows-Shropshire, S. I. Blum and M. Provencio Pulla, Perioperative Nivolumab in Resectable Lung Cancer, *N. Engl. J. Med.*, 2024, **390**, 1756-1769.
110. D. Miao, J. Zhao, Y. Han, J. Zhou, X. Li, T. Zhang, W. Li and Y. Xia, Management of locally advanced non-small cell lung cancer: State of the art and future directions, *Cancer Commun. (Lond.)*, 2024, **44**, 23-46.
111. G. Hardavella, A. Frille, R. Chalela, K. B. Sreter, R. H. Petersen, N. Novoa and H. J. de Koning, How will lung cancer screening and lung nodule management change the diagnostic and surgical lung cancer landscape?, *Eur. Respir. Rev.*, 2024, **33**, 230232.
112. G. Yang, S. B. Lu, C. Li, F. Chen, J. S. Ni, M. Zha, Y. Li, J. Gao, T. Kang, C. Liu and K. Li, Type I macrophage activator photosensitizer against hypoxic tumors, *Chem. Sci.*, 2021, **12**, 14773-14780.
113. H. Liu, J. Guo, W. Yin, H. Xiong, L. Chen, Y. Ruan, K. Feng, D. Su, Y. Liu and X. Sun, Dual-Locked Nanophotosensitizer Harnessing Cerenkov Radiation for Deep Tumor Therapy, *J. Med. Chem.*, 2025, **68**, 21988-21997.
114. E. D. Beffa, P. Lyberis, G. L. Rosboch, A. Arezzo, F. Lococo, L. Carena, E. Sciorsci, V. Monica, P. O. Lausi, V. Dusi, F. P. Busardò, E. Buffa, R. Stefania, G. Ciccone, C. Monagheddu, B. M. Capello, R. Vancheri, P. Garrone, F. Gabbarini, F. Cattel, E. Ruffini and F. Guerrero, Study protocol for Near-infrared molecular imaging for lung cancer detection and treatment during mini-invasive surgery (phase II Trial) - (the RECOGNISE study), *BMC cancer*, 2024, **24**, 1078.
115. H. Chen, H. Cheng, Q. Dai, Y. Cheng, Y. Zhang, D. Li, Y. Sun, J. Mao, K. Ren, C. Chu and G. Liu, A superstable homogeneous lipiodol-ICG formulation for locoregional hepatocellular carcinoma treatment, *J. Control. Release*, 2020, **323**, 635-643.
116. X. Yang, Y. Wang, C. Qu, B. Tan, M. Wang, S. Li, J. Huang, J. Li, M. Fang, Z. Cheng and N. Zhou, Real time monitoring peripheral nerve function with ICG and BDA-ICG by NIR-II fluorescence imaging, *Mater. Today Bio.*, 2024, **26**, 101084.



117. Y. Zhan, F. Song, W. Zhang, T. Gong, S. Zhao and F. Lv, Prediction of benign and malignant pulmonary nodules using preoperative CT features: using PNI-GARS as a predictor, *Front. Immunol.*, 2024, **15**, 1446511. View Article Online
DOI: 10.1039/D6SC02520J
118. F. Azari, R. P. J. Meijer, G. T. Kennedy, A. Hanna, A. Chang, B. Nadeem, A. Din, A. Pèlerin, B. Framery, F. Cailler, N. T. Sullivan, J. Kucharczuk, L. W. Martin, A. L. Vahrmeijer and S. Singhal, Carcinoembryonic Antigen-Related Cell Adhesion Molecule Type 5 Receptor-Targeted Fluorescent Intraoperative Molecular Imaging Tracer for Lung Cancer: A Nonrandomized Controlled Trial, *JAMA Netw. Open*, 2023, **6**, e2252885.
119. B. Zheng, Y. Chen, L. Niu, X. Zhang, Y. Yang, S. Wang, W. Chen, Z. Cai, W. Huang and W. Huang, Modulating the tumoral SPARC content to enhance albumin-based drug delivery for cancer therapy, *J. Control. Release*, 2024, **366**, 596-610.
120. L. Yin, P. Xu, Y. Huang, X. Gu, L. Sun, H. Zhou, W. Zhou, C. Xie and Q. Fan, Glutathione-Responsive Near-Infrared-II Fluorescence Probe for Early and Accurate Detection of In Situ and Metastatic Tumors, *Small*, 2025, **21**, e2503257.
121. K. Gu, Y. Xu, H. Li, Z. Guo, S. Zhu, S. Zhu, P. Shi, T. D. James, H. Tian and W. H. Zhu, Real-Time Tracking and In Vivo Visualization of β -Galactosidase Activity in Colorectal Tumor with a Ratiometric Near-Infrared Fluorescent Probe, *J. Am. Chem. Soc.*, 2016, **138**, 5334-5340.
122. Y. Zhang, Z. Li, H. Ge, X. Zhu, Z. Zhao, Z.-q. Qi, M. Wang and J. Wang, Dual hepatocyte-targeting fluorescent probe with high sensitivity to tumorous pH: Precise detection of hepatocellular carcinoma cells, *Sens. Actuators B Chem.*, 2019, **285**, 584-589.
123. M. Zhang, Y. Shen, X. Cheng, L. Yang, H. Li, Y. Tian and X. Tian, Engineering a tumor-specific and mitochondria targeted fluorescent probe for modulated autophagy and exploited anti-cancer therapy, *Sens. Actuators B Chem.*, 2022, **353**, 131178.
124. Q. Wang, L. Fu, Y. Zhong, L. Xu, L. Yi, C. He, Y. Kuang, Q. Huang and M. Yang, Research progress of organic fluorescent probes for lung cancer related biomarker detection and bioimaging application, *Talanta*, 2024, **272**, 125766.
125. E. Petrozziello, A. Sayed, J. A. Freitas, C. Federle, J. Nedjic, S. Ravens, B. Akçabozan, A. M. Schulz, D. Zehn, M. Schmidt-Supprian, R. Obst, I. Prinz, M. Verdoes, J. Kisielow, T. Reinheckel, T. Straub, S. R. Daley and L. Klein, Cathepsin L-dependent positive selection shapes clonal composition and functional fitness of CD4(+) T cells, *Nat. Immunol.*, 2025, **26**, 1127-1138.
126. X. Zhou, H. Chen, D. Huang, G. Guan, X. Ma, W. Cai, J. Liao and T. Guan, Reduced expression of cathepsin F predicts poor prognosis in patients with clear cell renal cell carcinoma, *Sci. Rep.*, 2024, **14**, 13556.
127. T. Zhan, J. Betge, N. Schulte, L. Dreikhausen, M. Hirth, M. Li, P. Weidner, A. Leipertz, A. Teufel and M. P. Ebert, Digestive cancers: mechanisms, therapeutics and management, *Signal Transduct. Target. Ther.*, 2025, **10**, 24.
128. S. Y. Yang, S. H. Li, J. L. Liu, X. Q. Sun, Y. Y. Cen, R. Y. Ren, S. C. Ying, Y. Chen, Z. H. Zhao and W. Liao, Histopathology-Based Diagnosis of Oral Squamous Cell Carcinoma Using Deep Learning, *J. Dent. Res.*, 2022, **101**, 1321-1327.
129. Z. Huang, Q. Jiang, Q. Zhang, N. Lu, X. Rui, R. Chen, Y. Wang, Y. Wang, X. Xu and Z. Huang, Neoadjuvant Chemotherapy With Cisplatin Up-Regulates GSDMD to Enhance Oral Squamous Cell Carcinoma Metastasis Through MMP14-Mediated EMT Activation, *Adv. Sci.*, 2025, **12**, e2501149.



130. V. R. Sahni, S. Chopra and A. Bharthuar, Is there a role of functional endoscopic evaluation of swallowing (FEES) in aiding tracheotomy decannulation post oral cancer surgery?, *J. Clin. Oncol.*, 2020, **38**, e18523-e18523. View Article Online
DOI: 10.1039/D6SC02520J
131. H. K. Yang and F. Berlth, Gastric cancer surgery: the importance of technique and not only the extent of lymph node dissection, *Lancet Oncol.*, 2019, **20**, 329-331.
132. F. Rosa and S. Alfieri, Laparoscopic Gastrectomy for Locally Advanced Gastric Cancer, *JAMA Surg.*, 2022, **157**, 545-546.
133. A. O. Andersen, A. Christensen, K. Straede, M. Lawaetz, C. H. Hahn, N. Rubek, I. Wessel, G. Lelkaitis, K. Kiss, N. Paaske, A. Poulsen, C. von Buchwald and A. Kjaer, Optical molecular imaging in oral- and oropharyngeal squamous cell carcinoma using a novel uPAR-targeting near-infrared imaging agent FG001 (ICG-Glu-Glu-AE105): An explorative phase II clinical trial, *Theranostics*, 2025, **15**, 52-67.
134. N. E. Burr, A. Plumb, R. Sood, B. Rembacken and D. J. M. Tolan, CT colonography remains an important test for colorectal cancer, *Gut*, 2022, **71**, 217-218.
135. N. S. Van Roermund, J. E. G. Ijspeert and E. Dekker, Developing a Strategy for Prevention of Avoidable Postcolonoscopy Colorectal Cancers: Current and Future Perspectives, *Gastroenterology*, 2025, **168**, 854-858.
136. K. M. Chan, K. Vasilev and M. MacGregor, Effects of Supplemental Drugs on Hexaminolevulinate (HAL)-Induced PpIX Fluorescence in Bladder Cancer Cell Suspensions, *Int. J. Mol. Sci.*, 2022, **23**, 7631.
137. M. M. Leitao, Jr., U. S. Kreaden, V. Laudone, B. J. Park, E. P. Pappou, J. W. Davis, D. C. Rice, G. J. Chang, E. C. Rossi, A. E. Hebert, A. Slee and M. Gonen, The RECURSE Study: Long-term Oncologic Outcomes Associated With Robotically Assisted Minimally Invasive Procedures for Endometrial, Cervical, Colorectal, Lung, or Prostate Cancer: A Systematic Review and Meta-analysis, *Ann. Surg.*, 2023, **277**, 387-396.
138. O. McKay, N. Shahidi, S. Gupta, W. A. van Hattem, T. El-Khoury and M. J. Bourke, Is it time to consider prophylactic appendectomy in patients with serrated polyposis syndrome undergoing surveillance?, *Gut*, 2021, **70**, 231-233.
139. M.-O. Grimm, M. H. A. Hussain, A. Stenzl, T. Todenhöfer, G. P. Haas, J. Sugg, R. Brauner, M. Gross-Langenhoff and C. N. Sternberg, Association of local progression with deterioration of urinary symptoms and occurrence of genitourinary adverse events (AEs) in nonmetastatic Castration-Resistant Prostate Cancer (nmCRPC): Post hoc analysis of PROSPER, *Eur. Urol.*, 2021, **79**, S1738-S1739.
140. G. J. Netto, M. B. Amin, D. M. Berney, E. M. Compérat, A. J. Gill, A. Hartmann, S. Menon, M. R. Raspollini, M. A. Rubin, J. R. Srigley, P. Hoon Tan, S. K. Tickoo, T. Tsuzuki, S. Turajlic, I. Cree and H. Moch, The 2022 World Health Organization Classification of Tumors of the Urinary System and Male Genital Organs-Part B: Prostate and Urinary Tract Tumors, *Eur. Urol.*, 2022, **82**, 469-482.
141. E. J. Schafer, A. Jemal, D. Wiese, H. Sung, T. B. Kratzer, F. Islami, W. L. Dahut and K. E. Knudsen, Disparities and Trends in Genitourinary Cancer Incidence and Mortality in the USA, *Eur. Urol.*, 2023, **84**, 117-126.
142. Z. Y. Wu, H. J. Kim, J. W. Lee, I. Y. Chung, J. S. Kim, S. B. Lee, B. H. Son, J. S. Eom, S. B. Kim, G. Y. Gong, H. H. Kim, S. H. Ahn and B. Ko, Breast Cancer Recurrence in the Nipple-Areola Complex After Nipple-Sparing Mastectomy With Immediate Breast Reconstruction for Invasive Breast Cancer, *JAMA Surg.*, 2019, **154**, 1030-1037.
143. Z. Bennett, Q. Feng, J. Thibodeaux, G. Huang, J. Gao and B. Sumer, Abstract B31: Delineation of sentinel



- lymph nodes in athymic nude mice by systemically administered ultra-pH-sensitive micelles shows fluorescence intensity in metastatic nodes, *Clinical Cancer Research*, 2020, **26**, B31-B31.
144. J. R. van der Vorst, B. E. Schaafsma, F. P. Verbeek, M. Hutteman, J. S. Mieog, C. W. Lowik, G. J. Liefers, J. V. Frangioni, C. J. van de Velde and A. L. Vahrmeijer, Randomized comparison of near-infrared fluorescence imaging using indocyanine green and 99(m) technetium with or without patent blue for the sentinel lymph node procedure in breast cancer patients, *Ann. Surg. Oncol.*, 2012, **19**, 4104-4111.
145. F. Gao, Q. Xie, X. Ran, X. Zhao, M. Yang, K. Jiang, T. Mao, J. Yang, K. Li and H. Wu, Use of indocyanine green-human serum albumin complexes in fluorescence image-guided laparoscopic anatomical liver resection: a case series study (with video), *Surg. Endosc.*, 2024, **38**, 6938-6947.
146. M. I. Abdelhamid, A. A. Bari, M. I. Farid and H. Nour, Evaluation of axillary reverse mapping (ARM) in clinically axillary node negative breast cancer patients - Randomised controlled trial, *Int. J. Surg.*, 2020, **75**, 174-178.
147. M. Scaranti, E. Cojocaru, S. Banerjee and U. Banerji, Exploiting the folate receptor α in oncology, *Nat. Rev. Clin. Oncol.*, 2020, **17**, 349-359.
148. P. Dell'Oglio, P. Meershoek, T. Maurer, E. M. K. Wit, P. J. van Leeuwen, H. G. van der Poel, F. W. B. van Leeuwen and M. N. van Oosterom, A DROP-IN Gamma Probe for Robot-assisted Radioguided Surgery of Lymph Nodes During Radical Prostatectomy, *Eur. Urol.*, 2021, **79**, 124-132.
149. E. Mazzone, P. Dell'Oglio, N. Grivas, E. Wit, M. Donswijk, A. Briganti, F. V. Leeuwen and H. V. Poel, Diagnostic Value, Oncologic Outcomes, and Safety Profile of Image-Guided Surgery Technologies During Robot-Assisted Lymph Node Dissection with Sentinel Node Biopsy for Prostate Cancer, *J. Nucl. Med.*, 2021, **62**, 1363-1371.
150. J. Y. Lee, J. P. Thawani, J. Pierce, R. Zeh, M. Martinez-Lage, M. Chanin, O. Venegas, S. Nims, K. Learned, J. Keating and S. Singhal, Intraoperative Near-Infrared Optical Imaging Can Localize Gadolinium-Enhancing Gliomas During Surgery, *Neurosurgery*, 2016, **79**, 856-871.
151. S. Li, Y. Liu, T. Yang, M. Deng, D. Cheng and L. He, Lysosome-specific near-infrared fluorescent probe with large stokes shift for H₂S imaging in U87 cells and brain glioma mice, *Sens. Actuators B Chem.*, 2025, **426**, 137109.
152. T. Tao, G. Li, K. Zhou, Q. Pan, D. Wu, L. Lai, M. Gao, S. Li, L. Chen, R. P. S. Han, P. Luo and Y. Tu, Discovery of Fatty Acid Translocase CD36-Targeting Near-Infrared Fluorescent Probe Enables Visualization and Imaging-Guided Surgery for Glioma, *Anal. Chem.*, 2025, **97**, 3687-3695.
153. Y. Feng, H. Yan, X. Mou, Z. Yang, C. Qiao, Q. Jia, R. Zhang and Z. Wang, A Dual-Cascade Activatable Near-Infrared Fluorescent Probe for Precise Intraoperative Imaging of Tumor, *Nano Lett.*, 2024, **24**, 6131-6138.
154. L. Yang, L. Jiang, F. Xu, H. Zheng, M. Liu, P. Shi, S. Zhang and X. Song, Hydrogen sulfide activatable NIR-II fluorescent probe for highly specific imaging of breast cancer, *Sens. Actuators B Chem.*, 2023, **379**, 133251.
155. T. L. Rose and W. Y. Kim, Renal Cell Carcinoma: A Review, *Jama*, 2024, **332**, 1001-1010.
156. Q. Wu, H. Shao, W. Zhai, G. Huang, J. Liu, J. Calais and W. Wei, Molecular imaging of renal cell carcinomas: ready for prime time, *Nat. Rev. Urol.*, 2025, **22**, 336-353.
157. N. H. Chakiryan, L. R. Gore, R. R. Reich, R. L. Dunn, D. D. Jiang, K. A. Gillis, E. Green, A. Hajiran, L. Hugar, L. Zemp, J. Zhang, R. K. Jain, J. Chahoud, P. E. Spiess, B. J. Manley, W. J. Sexton, B. K. Hollenbeck and S. M. Gilbert, Survival Outcomes Associated With Cytoreductive Nephrectomy in



- Patients With Metastatic Clear Cell Renal Cell Carcinoma, *JAMA Netw. Open*, 2022, **5**, e2212347. [View Article Online](#)
DOI: 10.1039/D6SC02520J
158. S. Ghodoussipour, T. Bivalacqua, R. T. Bryan, R. Li, M. C. Mir, J. Palou, S. P. Psutka, D. Sundi, M. D. Tyson and B. A. Inman, A Systematic Review of Novel Intravesical Approaches for the Treatment of Patients with Non-muscle-invasive Bladder Cancer, *Eur. Urol.*, 2025, **88**, 33-55.
159. J. Q. Chen, L. A. Salas, J. K. Wiencke, D. C. Koestler, A. M. Molinaro, A. S. Andrew, J. D. Seigne, M. R. Karagas, K. T. Kelsey and B. C. Christensen, Immune profiles and DNA methylation alterations related with non-muscle-invasive bladder cancer outcomes, *Clin Epigenetics*, 2022, **14**, 14.
160. A. Tosi, B. Parisatto, E. Gaffo, S. Bortoluzzi and A. Rosato, A paclitaxel-hyaluronan conjugate (ONCOFID-P-B™) in patients with BCG-unresponsive carcinoma in situ of the bladder: a dynamic assessment of the tumor microenvironment, *J. Exp. Clin. Cancer. Res.*, 2024, **43**, 109.
161. P. P. Avolio, R. Kool, B. Shayegan, G. Marcq, P. C. Black, R. H. Breau, M. Kim, I. Busca, H. Abdi, M. Dawidek, M. Uy, G. Fervaha, F. L. Cury, R. Sanchez-Salas, N. Alimohamed, J. Izawa, C. Jeldres, R. Rendon, R. Siemens, G. S. Kulkarni and W. Kassouf, Effect of Complete Transurethral Resection on Oncologic Outcomes After Radiation Therapy for Muscle-Invasive Bladder Cancer, *Int. J. Radiat. Oncol. Biol. Phys.*, 2025, **121**, 317-324.
162. H. Yan, X. Zhou, X. Wang, R. Li, Y. Shi, Q. Xia, L. Wan, G. Huang and J. Liu, Delayed (18)F FDG PET/CT Imaging in the Assessment of Residual Tumors after Transurethral Resection of Bladder Cancer, *Radiology*, 2019, **293**, 144-150.
163. Z. He, C. Wang, K. Song, L. Wang, K. Zhang, Y. Shi, X. Zhou and W. Shang, DDR-1 targeted fluorescent contrast agents for enhanced near-infrared tumor imaging, *Sens. Actuators B Chem.*, 2025, **433**, 137475.
164. Y. Ji, Q. Huang, Q. Jia, H. Yan, Y. Chi, Y. Jia, C. Qiao, Y. Feng, Z. Yang, R. Zhang and Z. Wang, A H2S-activated NIR-II imaging probe for precise diagnosis and pathological evaluation of colorectal tumor, *Theranostics*, 2025, **15**, 189-201.
165. H. Li, Q. Yao, W. Sun, K. Shao, Y. Lu, J. Chung, D. Kim, J. Fan, S. Long, J. Du, Y. Li, J. Wang, J. Yoon and X. Peng, Aminopeptidase N Activatable Fluorescent Probe for Tracking Metastatic Cancer and Image-Guided Surgery via in Situ Spraying, *J. Am. Chem. Soc.*, 2020, **142**, 6381-6389.
166. Q. Wu, Q. H. Zhou, W. Li, T. B. Ren, X. B. Zhang and L. Yuan, Evolving an Ultra-Sensitive Near-Infrared β -Galactosidase Fluorescent Probe for Breast Cancer Imaging and Surgical Resection Navigation, *ACS Sens.*, 2022, **7**, 3829-3837.
167. K. Yang, S. Fan, J. Wang, L. Yin, Z. Li, S. Xiong, G. Han, C. Meng, P. Zhang, X. Li and L. Zhou, Robotic-assisted Lingual Mucosal Graft Ureteroplasty for the Repair of Complex Ureteral Strictures: Technique Description and the Medium-term Outcome, *Eur. Urol.*, 2022, **81**, 533-540.



Data Availability Statement

The figures used in this review are available from the respective publications and are reproduced with permission. The original sources and related information for the figures can be found in the reference list.

